This is a preprint, the final version is subject to change, of the American Mineralogist (MSA)
Cite as Authors (Year) Title. American Mineralogist, in press.
(DOI will not work until issue is live.) DOI: http://dx.doi.org/10.2138/am.2013.4388 7/11

Revisions

A study of ruby (corundum) compositions from the Mogok belt, Myanmar: Searching for chemical fingerprints

George E. Harlow[1,*] and Will Bender[2]

[1]Dept. Earth & Planetary Sciences, American Museum of Natural History, New York, NY 10024-5192, U.S.A.

[2]Whitman College, Walla Walla, WA 99362, U.S.A.

* Present address: Department of Earth & Planetary Sciences, American Museum of Natural History, New York, NY 10024-5192, U.S.A. E-mail: gharlow@amnh.org

ABSTRACT

For centuries the Mogok metamorphic belt of Myanmar (a.k.a. Burma) has been famous for producing classic, pigeons-blood ruby (corundum: Al_2O_3) specimens. The present model for the formation of rubies hosted in marble from the Himalayan arc is a closed-system metamorphism of former clays from evaporitic/organic-rich shale units in margin basins. Mogok has still not been fully included in this model. Involvement of igneous intrusions and the formation of skarn with the marble has been an outstanding topic. Twenty three red corundum samples (nominally rubies) from eight sources in the Mogok belt marbles, including a skarn setting and local alluvial samples, have been analyzed using the electron microprobe and a laser-ablation inductively-coupled plasma mass spectrometer system in order to measure trace element compositions for evidence of different geological formational environments. Although inclusions, such as baddeleyite (ZrO_2) and srilankite ($[Ti,Zr]O_2$), as well as

associated painite ($CaZrAl_9O_{15}[BO_3]$), indicate skarn-related paragenesis of some samples, no signatures of B or Zr enrichment were found. Rather high levels of Si (300+ ppm) are found, possibly indicating nano-silicate inclusions when above 500 ppm. A distinct Fe enrichment, as in the case of metasomatic ruby, is observed. Sensitivity to the sub-ppm level may to be necessary to resolve, if even possible, whether there is a compositional signature from the skarn formation. Samples from individual sources in the belt show some distinct trace-element characteristics, in particular a discretely limited variation in V/Ti while the Cr content can vary considerably and independently. With the potential of V, Ti, and Cr being sourced from blackshale components in shelf carbonates that were transformed to marble, these Mogok belt rubies may record an informative intersection of organic chemistry, geochemistry, plate tectonics, metamorphism and metasomatic processing.

Keywords: ruby, corundum, Mogok, Myanmar, chemical compositions, geological source

INTRODUCTION

For centuries the Mogok Stone Tract of Myanmar (a.k.a. Burma) has been held as one of the quintessential sources for fine rubies. However, a consensus on the formation conditions of the Mogok ruby has yet to be reached (Giuliani *et al.* 2007). Although the Mogok Marble Belt is recognized as the host for the rubies, in light of the complicated geological setting many different hypotheses have been developed to explain the occurrence of the pigeon-blood red corundum. These hypotheses include metamorphism of the aluminous component of carbonate sediments, metasomatic reactions involving ultra-saline hydrous fluids, pneumatolytic reactions from granite bodies, and, finally, reactions in the formation of skarn or tactite (Giuliani *et al.* 2007; Iyer 1953; Harlow *et al.* 2006). Garnier *et al.* (2008) have reviewed the models and proposed a largely closed-system of metamorphic origin for many of the marble-hosted ruby sources from platform carbonate deposits in southern Asia. However, they hesitated in extending the model to the Mogok and Mongshu deposits in Myanmar for lack of sufficient data on them. The Mogok belt evidences considerable tectono-magmatic activity through world-class rare-element pegmatite mineralization (beryl or LCT type: Thu 2007) with local mines producing ruby, spinel, and pegmatite minerals. Thus, a combination or hybridization of parageneses may be applicable to different areas of the Mogok region. The finding of ruby overgrowths on painite ($CaZrBAl_9O_{18}$) + tourmaline (mostly foitite, less dravite and uvite) clearly supports at least one instance of skarn-formed ruby (Nissinboim and Harlow 2011), so a close examination and comparison of the ruby from the Mogok Belt was considered worthwhile (skarn here means a rock or assemblage formed by an igneous-rock–carbonate contact metasomatism, synonymous with tactite). Moreover, the availability of ruby samples collected at the sources permits greater specificity than is generally available in the literature, dominated by examination of cut stones or rough material amalgamated in lots without known sources.

Ruby, formed potentially by different growth processes and in different parts of the Mogok belt, may exhibit different trace element compositions. Thus, analysis of them may provide a "fingerprint" that could be associated with different paragenetic processes or sources. This study presents such data on multiple crystals of ruby from eight distinct sources in the Mogok belt, including ruby-on-painite from Wet Loo. These data are compared with results reported in the literature, although data reported in the gemological literature is often limited and not readily comparable since it is presented in plots and ranges rather than as discrete analyses.

GEOLOGICAL SETTING

The Mogok Belt is a part of the Shan Highlands, the elevated region along the east side of Myanmar. Some granulite gneisses in the belt have been interpreted as being Proterozoic (>750 Ma) with the overlying Chaung Magyi turbidite (shale-sandstone deposited on a continental slope via submarine mudflows—Late Proterozoic) and carbonates (limestones and Shan dolomite) of Permian to Triassic age (~250 - 200 Ma) (see Mitchell 1992, 1993). Metamorphism of these rocks was a multi-step process related to the closure of the Tethyan Oceans. First was the collision of a fragment (the Burma Plate) of the megacontinent Gondwanaland (the other relics were India, Australia and Indonesia) in Jurassic-to-early-Cretaceous time (150 Ma: Mitchell 1981, 1989) or perhaps as late as Late Cretaceous (90 Ma; Hutchison 1989). This was accompanied by intrusion of granites related to the tin-granite province continuing into Malaysia that become younger to the north. Subduction of the Tethys III Ocean produced mid-Cretaceous and younger intrusive rocks in the central valley of Burma which may have led to continuing metamorphism and metasomatism. Collision of the Indian subcontinent with SE Asia, coupled with the Himalayan orogeny in Eocene time, subducted continental sediments leading to intrusions of the two-mica tin-bearing granites into the Mergui

group of the Shan Plateau in late Mesozoic to Eocene time (produced by crustal thickening) and to considerable compression and uplift of the Shan highlands that bears the Mogok belt. Rotation of SE Asia clockwise by the Indian collision led to the Sagaing Fault that sheared off the eastern edge of the Mogok Belt along with the so-called Sibumasu terrane, leading to a displacement of marbles as much as 400 km between Namya (a.k.a. Nanyaseik), to the north adjacent to the Jade Mine Tract (see Mitchell 1989, 1992, 1993; Bertrand *et al.* 1999) and the main belt. E-W compression has led to recent uplift of the Shan Highlands, exposing the ruby-bearing marbles to erosion and creating the rich alluvial deposits from which most of the gems have been retrieved.

The focus of this research is the possibility of differentiating among crystallization processes of ruby. Knowing the ages of events, particularly for intrusions, should be informative. Radiometric dating by Bertrand *et al.* (2001) indicates that the latest regional metamorphism in this area occurred during the Late Oligocene to Early Miocene, about 20-25 Ma ago. ^{39}Ar-^{40}Ar dating of the Kabaing granite is ~16 Ma (Bertrand and Rangin 2003) and a U-Th-Pb age of uranothorite, from the related Sakhangyi pegmatite, is ~15 Ma (Searle and Haq 1964). U-Th-Pb zircon dates from the Pingutaung leucogranite (includes syenites) are 32±1 Ma for the igneous rock and 16.1±0.5 Ma from painite-bearing skarn at the contact between the leucogranite and marble (Thu 2007). Garnier *et al.* (2006) report ^{40}Ar-^{39}Ar cooling ages for phlogopite associated with ruby as 18.7 ± 0.2 to 17.1 ± 0.2 Ma, consistent with the ages of the earlier intrusives. So, clearly the painite crystallization postdates the most recent regional metamorphism.

Because the Wet Loo skarn is an important focus of interest in this research, and the citation is not readily available, the description in Thu (2007, p125-126) is useful here:

Primary deposits of painites from Wet-loo JV mine and Thurein Taung area mines suggests growth during skarn forming event between leucogranite and phlogopite marble,

associated with ruby. In this area, leucogranite intrusives are (in) faulted contact with phlogopite marble along the Wet-loo stream and Thurein Taung. The painite bearing contact zone is localized, about 3 to 6 m in width and upto 10m in length. Minerals associated with painite include ruby, scapolite, spinel, phlogopite, tourmaline, pyrite and margarite from Wet-loo mine and also ruby, scapolite, mica, pargasite, tourmaline, baddeleyite, anatase, sphene, pyrite and etc. from Thurein Taung area mines. The silicates are typical of skarns and argue for interaction between magmas (or their fluids) and marble. A conspicuous textural feature of these mineral assemblages is ruby crystallized on painite, demonstrating ruby growth during skarn formation. A detailed description of the painite specimens is part of ongoing research (e.g., tourmaline identification noted above), abstracted in (Nissinboim and Harlow 2011).

SAMPLES

Samples for this study (Table 1) were selected from the mineral collection at the American Museum of Natural History (AMNH), which contains over 300 appropriate specimens from Myanmar (the naming convention for translation of Burmese place names are taken from Themelis 2008). For this study we considered samples from intense red, thus "true" gemological ruby, to pink colors that do not fit a rigorous definition, but excluded we colorless samples or specimens of other colors. The ruby samples originate from mines and villages within the Mogok marble belt, including the Mogok Stone Tract (Figs. 1 & 2). The second author traveled to Myanmar several times between 1998 and 2002 and acquired samples, typically bags of individual crystals, from miners and dealers at or near the source. For example, samples from Namya, west of the Sagaing fault, were acquired from local villagers, while Sabaw samples were acquired at a local mine (mixed colluvial and marble-hosted samples) a few kilometers out of Namya. Mineral samples containing ruby crystals were sourced the same way or from dealers. Here the mineral assemblages helped confirm the source. The sector-

zoned trapiche ruby samples included in this study were originally recorded as coming from Thabeikkyin (see Fig. 1), but, upon checking again with the dealer from whom they were acquired, they come from the Mongshu area, where trapiche samples are reported (*e.g.*, Garnier *et al.* 2002. They are retained for comparison with data from both Myanmar source regions and designated as "Trapiches" in plots. Ultimately, 23 samples were selected to provide both a diversity of sources and duplication. They include representatives from the Mogok Tract proper, two sources associated with the Mogok belt away from Mogok but east of the Sagaing Fault, sources west of the fault near Namya, and the Mongshu trapiche crystals. Samples from Wet Loo consist of ruby coating painite crystals and originate from a contact zone between the leucogranite and the Mogok marble (Themelis 2008; Iyer 1953; see Fig. 2). All the deposits in this area are described as related to skarn formation, and the painite assemblage clearly indicates a skarn origin (Thu 2007, Nissinboim and Harlow 2011).

For this study, the goal was to select a representative group of samples from the more than 300 from the Mogok belt in the AMMH collection. To verify phase identification and any associated phases, samples were examined using X-ray diffraction. Most samples were hosted in calcite from the Mogok marble. Secondary phases include pyrite, pyrrhotite, sodalite, balliranoite (cancrinite-group), clinohumite, and montmorillonite (see Table 1). The clinohumite, in association with corundum, is F-rich, near the end-member composition. This is probably an indication of the influence of fluid interactions from an evolved igneous source (e.g., see Deer et al. 1982), although a strictly metamorphic origin for a fluorine-rich protolith cannot be ruled out. The assemblage sodalite, balliranoite, nepheline (or alkali feldspar), and the scapolite-series has also been found associated with ruby from the Mogok tract (*e.g.*, Dattaw, Kyauksin, and Wet Loo: Harlow *et al.* 2006; Themelis 2008) and may be the result of reactions between marble and the intrusives (or related fluids known from the tract). In addition to the

159 association of ruby and painite from Wet Loo, painite has been found in gravels at Namya
160 (Rossman *et al.* 2005).

161 Grain mounts suitable for cathode luminescence (CL), electron probe micro analysis
162 (EPMA), and laser ablation inductively-coupled plasma mass spectrometry (LA-ICPMS)
163 analysis were prepared by mounting specimen grains or fragments in epoxy in 1 inch cylinders.
164 These mounts were then ground on a 30-μm metalized diamond lap to expose grain cross
165 sections and then polished using a combination of silicon carbide and diamond lapping disks. In
166 total, 24 samples from 8 localities were prepared and analyzed (Table 1**).**

167 **ANALYTICAL METHODS**

168 **X-ray Diffraction**

169 Samples were examined, either as small areas of the whole crystal or minute fragments
170 from the whole grain, using a Rigaku DMax/Rapid X-ray microdiffraction system at the
171 AMNH. The system utilizes a narrowly collimated beam of X-rays to bathe a small sub-sample
172 (100 μm to 1 mm) or a similar size area on a sample, which rotates/oscillates about two axes to
173 produce a quasi-powder pattern on a cylindrical image plate, which then is converted into a
174 standard "2θ-Intensity" diffractogram. Typical operating conditions involved a 0.8 mm
175 collimator employing monochromated Cu Kα X-rays at 46 kV and 40 mA. Diffractograms
176 were interpreted using JADE (MDI) software and the ICDD PDF-2 diffraction database for
177 minerals and inorganic phases supplemented by our own library of patterns.

178 **Cathodoluminescence (CL) Electron Microscopy**

179 Ruby samples were observed with a Gatan Mono CL system mounted on a Hitachi S-
180 4700 Scanning Electron Microscope in the Microscopy and Imaging Facility at AMNH.
181 Samples were coated with a thin layer of carbon in a vacuum evaporator. Operating conditions
182 in the Hitachi were 5 kV at 5-10 nA sample current. Images were collected in panchromatic

mode with the goal of observing zoning that would otherwise be difficult to observe using more typical backscattered electron (BSE) images in a relatively pure phase like corundum.

Electron Probe Microanalysis (EPMA)

EPMA was carried out on a 5-spectrometer Cameca SX100 equipped with an Oxford/Esprit energy dispersive spectrometer (EDS) system at the Department of Earth and Planetary Science at AMNH. Operating conditions were 15-20 kV and 20-40 nA sample current. The elements analyzed for were Na, Mg, Al, Si, Ca, Ti, V, Cr, Mn, Fe, Zn, and Ga. Detection limits range from 29 to 615 ppm and are reported in Table 2. Natural and synthetic compound standards were used along with the PAP correction scheme of Pouchou and Pichoir (1991). Zinc, Ca, and Na were analyzed at 15 kV and 10 nA for 20 seconds. Since the scatter in values for these elements yields maximums that are likely higher than is reasonable, they are reported with a question mark in most cases in Table 2. Standard deviations by counting statistics for individual analyses of minor elements range from 10 to 350 ppm (Table 2). Most analyses were collected as traverses of 15-20 points over 1 – 6 mm on the crystals adjacent to LA-ICPMS traverses to provide comparable sets of compositional data. Inclusions in ruby were also examined on the SX100 with a combination of backscattered electron (BSE) imaging, EDS observation, and wavelength analysis, when applicable.

Laser-ablation inductively-coupled plasma mass spectrometry (LA-ICPMS) analysis

LA-ICPMS analysis was carried out in the ICPMS facility at Columbia University's Lamont-Doherty Earth Observatory in Palisades, NY. The instrument used is a VG PlasmaQuad Excell ICPMS with New Wave UP 193 FX excimer laser ablation microscope. The 193 nm laser was set to an irradiance of 1.51 Gw/cm^2 and a fluence of 7.55 J/cm^2. For standards the pre-ablation surface cleaning employed a 50 μ/sec scan at 20 percent laser power and 125 μm beam diameter. Standard measurements were made in traverses at 3 μm/sec at 70% laser power with a

100 μm beam diameter after a 60 second delay for establishing background. For measuring the ruby samples, the same procedure was performed, except that the delay was 30 seconds and the ablation was carried out at 10 μm/sec. Nineteen elements were selected for analysis based on the results of previous workers (*e.g.*, Abduriyim and Kitawaki 2006a,b; Guillong and Gunther 2001; Calligaro *et al.* 1999; Muhlmeister *et al.* 1998; Osipowicz *et al.* 1995; Tang *et al.* 1988). The potential for observing the effects of an evolved magma, rich in lithophile elements, or common to painite: ^{7}Li, ^{9}Be, ^{11}B, ^{24}Mg, ^{27}Al (internal standard), ^{29}Si, ^{43}Ca, ^{44}Ca, ^{47}Ti, ^{51}V, ^{52}Cr, ^{55}Mn, ^{57}Fe, ^{65}Cu, ^{66}Zn, ^{69}Ga, ^{90}Zr, ^{93}Nb, ^{118}Sn, ^{120}Sn(Te), ^{138}Ba, and ^{181}Ta; detection limits are reported in Table 3. Counting data were converted into concentrations using an Excel macro/program called LASY BOY (Sparks 2001).

RESULTS

CL

In previous studies of ~~the~~ Mogok samples, ruby has shown visible zonation features (Harlow *et al.*, 2005). However, for the majority of samples in the sample suite chosen for this study, no significant features were detected in CL. The homogenous samples were very faintly luminous and in some cases, were even hard to distinguish from the epoxy.

Trapiche ruby samples from Mongshu (110343) showed the most pronounced, although subtle, zonation features (Fig. 4a). The zoning bands are parallel to the external prismatic face of the trapiche crystal (presumably the (112$\bar{0}$)). A crystal in a calcite (marble) matrix from Dattaw (107643) shows a bright band at 670 nm at the corner of the crystal (Fig. 4b), which is clearly associated with a higher Cr content (see below).

EPMA

EPMA analytical results are summarized in Table 2 as ranges over the transects on each sample. Complete analyses are given in Appendix 2. Elements consistently above detection

limits included Ti, Cr, V, and Ga. Values for Mg, Fe, and Mn are less consistently above background, and values for Zn, Ca, and Na are questionable when they exceed 100 ppm. Silicon is clearly found in all samples above the detection limit of about 65 – 100 ppm. It ranges from ~500 ppm to much higher and sporadic values (>1000 ppm) suggesting microinclusions that were not visible with a binocular microscope (discussed below). Wavelength scans confirmed that a Si "peak" exists. Corundum samples analyzed by EPMA in other studies have shown low Si, but generally higher than in this study (e.g., Garnier *et al.* 2002: in Mongshu trapiche ruby 0.02-0.06 wt% SiO_2 [= 900 – 2800 ppm] but the significance was not discussed), or have been below detection limits (Sutherland *et al.* 1998). Inclusion phases detected with BSE and evaluated by EDS and WDS are presented in Table 1 and Appendix 2. Of note are inclusions of baddeleyite and srilankite in crystals not associated with painite or a skarn source.

As the EPMA resolution is much finer than LA-ICPMS analysis, zoning variations, when present, are much more clearly resolved (see Table 2). The most common growth zoning is a band structure (e.g., 11224 Trv1, 109270 Trv1) or a rim concentration (e.g., 107643, 108498 Trv3). The greatest variation is in Cr abundance. However some covariation of V, Ti, Fe, (e.g., 109272-2, 109274-2), and counter variation of Cr with Ti, Fe, and perhaps Mg is observed (110343-3). The trapiche ruby crystals from Mongshu show the largest variation in growth zoning (see Fig 5).

LA-ICPMS

The LA-ICPMS data are summarized in Table 3. Trace elements consistently above the detection limits are Ti, V, Cr and Ga. Other elements that are above the detection limits for several of the 55 compositional integrations include Be, Ta, Nb, Zr, Zn, and Mg. Boron, Fe, Ca, Cu, and Ba are above the detection limit for only a couple of analyses. Lithium and Mn are never above the detection limit. Mass interferences account for the poor detection of Fe and Si. Concentrations of Ti, V, Cr and Ga provided the basis for comparison with other published data,

bolstered by the EMP data. In many other studies of corundum trace elements, Fe has been detected at higher concentrations than in our corundum samples (e.g., for non-Burma-ruby 300-4130 ppm—Calligaro *et al.* 1998; 70-12980 ppm—Muhlmeister *et al.* 1998; 210-10990 ppm—Rankin *et al.* 2003). However, Mogok rubies are generally low in Fe (*e.g.*, all but one sample here excluding the Sagyin and Wet Loo samples are < 300 ppm by microprobe—see Fig. 6a, consistent with the literature), so our detection limits for Fe with LA-ICPMS (typically >390 ppm) were too high to detect the small concentrations present.

Comparison of EPMA and LA-ICPMS Results

For the elements that were analyzed by both techniques, there is a general consistency, but differences should be pointed out. Because of the detection problems with Si and Fe in our LA-ICPMS analysis, values for these two elements can only be assessed with the EPMA data. Whereas Ga values overlap for the two techniques, the range and number of EPMA values are nearer to 100-200 ppm compared to 10-100 ppm for LA-ICPMS. Analyses for Zn by EPMA, which were not uniformly collected, appear to be too high if above the detection limit, particularly when compared to either Fe content or values from LA-ICPMS. A possible explanation is that Zn resides in micro-inclusions, rather than in the corundum structure because the sample with the highest integrated values for both techniques is 108498 from Kadoke Tat. This sample also contains pyrrhotite inclusions, which might indicate another phase such as sphalerite (see Table 1 & 2). Magnesium is another element at levels near the detection limit for both techniques but shows consistent elevation ~≥100 ppm in 109270 from Sagyin using both techniques.

Compositional characteristics by locality

Previous studies of ruby and sapphire have focused on discriminating among broadly different origins and to some extent individual sources among a single category, such as marble-

hosted ruby, which has been the categorization for ruby of the Mogok metamorphic belt. We follow this approach but also break out the separate sources and the variation among samples from each source. The localities are organized from east, well within the Mogok stone tract, southwestward, and finally to the separated area of the Mogok belt near Namya (Figs. 1 and 2).

Dattaw: The two samples from this locality, known for large crystals in matrix associated with scapolite, colorless sodalite, and blue balliranoite, contain moderately low Cr, generally < 200 ppm, but with evidence of an increase at the crystal edges to > 100 ppm in otherwise unzoned crystals. Vanadium is likewise somewhat low, but other elements are not notably different from other samples.

Wet Loo: The two samples examined are overgrowths on corundum with tourmaline on painite (Nissinboim and Harlow 2011) and so do not represent potential gem rough. The grains generally have two different levels of trace elements in apparent band-like zoning. These zones most conspicuously have different levels of Cr. The lower level is ~700-800 ppm and the other is 1100-1500, and less noticeably corresponding V at ~200 and ~320 ppm, respectively. Conspicuously, EPMA shows relatively high Fe (300-700 ppm) and generally high Si (270-500 ppm) with some much higher Si analyses (>1000 ppm), plotting as a distinct group (see Fig. 6A). As the very high Si values are individually discontinuous with respect to traverse position points, we assume they result from micro inclusions.

Kadoke Tat: Both samples are clusters of crystals in a marble matrix and show variability between the different portions analyzed. Sample 108498 manifests subtle zoning with relatively high Cr (1200-1700 ppm vs. 2000-4000 ppm) followed by V (190 – 230 vs. 270 – 350 ppm) without clear relationship to other elements. One traverse from LA-ICPMS analysis showed a zone of detectable Be, Zn, Sn, Mg, and high Fe and Cu, (traverse 108498-1c; Table 3). This may represent incorporation of a sulfide inclusion in the analysis (pyrrhotite was observed as an

inclusion in corundum in another part of the sample). EMPA adjacent to this traverse manifested inverse zoning between Cr (2000 – 2350 vs. 1500 – 1700 ppm) and Ti (~50 vs. ~150 ppm), Mg (~bdl vs. ~50 ppm), and Fe (~60 vs. 100 – 200 ppm). Sample 108502 contains generally less Cr but is also zoned (~200 to 2000 ppm) that appears locally inversely correlated with V and Ti in the LA-ICPMS (Table 3) traverse. This relationship is less clear in the EMPA data, although it is clear that V lies at higher contents than the typical Cr-V trend of the rest of the samples (Fig. 6B) while Ti levels are generally low, i.e. ≤ 100 ppm.

Kyauksin: This single sample showed evidence of having been dyed, as the sample mount showed mare's tail stains emanating from the ruby-marble contact into the epoxy mounting resin. The traverses do not show zoning and are relatively low Cr and Ti, similar to the Dattaw samples but with slightly more V (Fig. 6B).

***Sagyin*:** Five grain samples and one matrix one from Sagyin, where marble quarries area contain ruby and spinel grains, are included in this study. As a group they have moderate amounts of most measured elements, but with the greatest range in Fe, as high as in the Wet Loo samples but with slightly more Ti (Fig. 6C) and less Si (Fig. 6A). All but one, 112703, are zoned, which typically features Cr enrichment near the grain rim. Zoning includes inverse concentrations of Cr (500 to 2500 ppm) and V versus Ti (325 to 230 ppm) in 109270 (only EMPA) or high versus low for all three. Gallium may be enriched in a band in 112704 from <80 ppm to ~200 ppm, but precision does not permit a clear distinction.

***Namya and Sabaw*:** Trace elements are in the middle to higher range for the Mogok-belt group excluding Wet Loo and Thabeikkyin. Individual grains can contain relatively low Cr, V, and Ti (e.g., 109276-1) or higher contents (109274-3). A few individual points in traverses have a high Si content suggesting silicate micro-inclusions as seen in the Wet Loo corundums. Painite has also been found as small pebbles at Namya.

Mongshu: As pointed out previously, these three trapiche ruby crystals show considerable core to rim zoning and contain the most Cr and Ti as a group. The highest Cr, V, and Ti are found in the dark red crystal 110343-1 (Fig. 6C). Two of these three samples contain Be above the detection limit and one (110343-1) had the highest measured level (5.7 ppm) of all samples.

DISCUSSION

Comparison with published data

From the extant studies on rubies by PIXE (proton-induced X-ray emission: Tang *et al.* 1988, 1989; Osipowicz *et al.* 1995; Sanchez *et al.* 1997; Calligaro *et al.* 1998, 1999), by LA-ICPMS (Rankin *et al.* 2003), by energy-dispersive X-ray fluorescence (EDXRF: Peretti *et al.*, 1995; Muhlmeister *et al.* 1998), and by EPMA (Garnier *et al.* 2002), the discriminants most used, when comparing sources, have been binary and ternary plots of the significant minor elements Cr, Ti, Fe, and Ga. We follow this practice as well, because most of the data from the gemological literature tends to be compilations only with averages and ranges published, or binary or ternary plots in terms of the four elements. Consequently, some of our comparisons with the groupings described below are inferred from a few averages and points derived from the literature. Tang *et al.* (1988, 1989, 1991) published a considerable amount of data, however, it has been pointed out by Osipowicz *et al.* (1995), there may be systematic errors in their estimates of Fe (and Si), many being higher than those of other researchers. Consequently, we have not used any Tang *et al.* data in our comparisons except for basalt-hosted rubies.

Calligaro *et al.* (1999) and Rankin *et al.* (2003) were able to distinguish ruby samples from different formational environments based on a Fe versus Cr plot, onto which we have plotted the EMPA data in Fig. 7A. This plot shows that ruby samples cluster as three broad elliptical distributions: Group I – metamorphic (marble hosted), generally defined by low Fe; Group II – metasomatic/metamorphic (fluid interactions with host rock); and Group III –

353 basaltic (see also Muhlmeister *et al.* 1998; Giuliani *et al.* 2007, 2012). It should be pointed out
354 that Group II is a catch all group which does not truly distinguish between metamorphic,
355 metasomatic and igneous origin, rather the origin is just neither marble nor basalt. Calligaro *et*
356 *al.* (1999) imply that V provides a third component for discrimination but do not provide a plot,
357 so we have interpreted from the limited data provided in this paper as well as Calligaro *et al.*
358 (1998). Chromium vs. V and V vs. Fe plots are shown in Figs. 6B and 7B, respectively. The
359 plots are all consistent in showing most of the Mogok belt rubies studied here to be Group I
360 with some overlap into Group II, particularly Wet Loo and some Sagyin, and with a greater
361 range in Cr.

362 Another approach at distinguishing origin via a trace-element plot is the V-Fe-Ga plot of
363 Muhlmeister *et al.* (1998), here including data of Calligaro *et al.* (1998, 1999), Peretti *et al.*
364 (1995), and Osipowicz *et al.* (1995) for Mongshu, with our EMPA data for comparison in Fig.
365 8A. Clearly this comparison shows the consistency of the absence of the high Fe rubies (Group
366 II and Group III) for most Mogok belt "rubies", but with the Wet Loo, Dattaw, and Sagyin
367 samples showing relatively high Fe relative to the Group I cluster. The higher values of Ga in
368 our data may represent a systematic error. This is because estimates appear to be too high in the
369 EMPA data, as the LA-ICPMS values are generally lower with Ga < V (Fig. 8B). Consequently,
370 it is more likely that the EPMA data should be adjusted to plot in the upper left portion of the
371 triangle, comparable to the published XRF and PIXIE data. Guillong and Gunther (2001) used a
372 V-Fe-Ga plot to sort among different origins of sapphires. However, they normalized the data to
373 the standard deviation of each element throughout the data set. Consequently, geologically
374 valuable compositional information is obscured, and such an approach has not been followed
375 for our data. Another plotting scheme uses Fe_2O_3/Cr_2O_3 vs. Cr_2O_3/Ga_2O_3 , originally used by
376 Sutherland *et al.* (1998) to distinguish metamorphic from igneous-hosted corundum and by
377 Schwarz and Schmetzer (2001) and Rankin *et al.* (2003) for rubies. As Ga variation among

marble-hosted ruby is small, this plot has no advantage over the Cr vs. Fe plot. Moreover, with the unresolved Ga values from EPMA data, comparisons with published plots would be questionable.

A ternary V-Cr-Ti plot of the ruby data (Fig. 8C) shows an interesting pattern of data aligning along bands of relatively constant V/Ti ratio, with the highest for Kadoke Tat and lowest for Mongshu, both published and these data. In particular individual samples show this characteristic and, then, samples from a single locality tend to cluster with a limited range in V/Ti. This relationship was noted by Rossman (2009) for differentiating Mongshu rubies from other marble-hosted sample in his review of the geochemistry of gem minerals. Clearly, the Cr variation appears to be somewhat independent of this compositional variation, other than the fact that Cr is always present at some level. In addition, the greater variability in V/(Cr+V) (Fig. 6B), as exemplified by data for Kadoke Tat, Kyuaksin, and even Dattaw, compared to the published data, is noteworthy.

Criteria for recognizing metasomatic from metamorphic rubies the Mogok belt

The rationale for this study was to seek signatures in ruby chemical composition for crystallization during skarn formation of corundum on painite at Wet Loo, or the less clear relationships of specimens from Dattaw and Kyauksin. Thus, it is necessary to discuss in a little detail the latest model and consequences thereof for ruby formation in the marbles of Mogok and southeast Asia in general. Garnier *et al.* (2008) have presented comprehensive evidence for an origin from metamorphism, through the Himalayan orogenesis, of platform carbonate deposits containing organic-rich evaporites. Significantly, for this study, they do not find evidence for the effects of igneous interactions, whether of some general metasomatic type (a fluid interaction or replacement) or of the specific skarn (igneous contact and interaction with marble) formation (*e.g.*, Iyer 1953; Harlow *et al.* 2006; Nissinboim and Harlow 2010). The reason, largely, is that both the carbon and oxygen isotopic signatures of all the samples they

studied reflect that of the hosting marble, although they acknowledge that their data on the Mogok belt rubies and geology are inadequate to extend the model directly there. The point here is not to challenge this model but to look for evidence of the igneous interactions in the compositions of the corundum that might reflect the elements that are involved with the formation of painite, tourmaline (foitite-uvite-dravite series), sinhalite, baddeleyite, etc. (Nissinboim and Harlow 2010; Thu 2007) and be used as a diagnostic for ruby of similar origin. This study of Mogok belt rubies was unable to consistently detect elements such as B, Be, Zr or Li(?) that are key constituents in the minerals noted above or consistent with highly evolved granitic fluids. These elements are not expected to be compatible on crystallochemical grounds (*i.e.*, ionic radius and charge), so concentrations were anticipated to be very low. Our detection limits for these elements range from 0.2 to 53 ppm (see Table 3), so it is possible that a lower detection limit would provide the needed resolution to show the compositional effect of an equilibrium assemblage of corundum with painite, baddeleyite, and tourmaline. Other researchers have published values for some or all of these elements in corundum (Schwarz *et al.* 2008; Guillong and Gunther 2001) with the greatest sensitivity in the range of 1.6 to 3.6 ppm for B or 0.01 to 0.29 ppm for Zr by LA-ICPMS, but these data have not been interpreted. Alternatively, perhaps the corundum formed later, by a metasomatic event affecting the skarn after it had already formed, and thus will not have a clear signature of the skarn reactions. However, the finding of ruby both within as well as on painite (Nissinboim and Harlow 2010) should preclude this interpretation.

Nonetheless, the corundum samples intergrown with painite do have compositions that depart from both the Group I classification and many of the other samples in our study. The first distinguishing feature noted is the relatively high Fe content (>300 ppm) and Si content (>300 ppm) obvious in Fig. 6A. Higher Fe is generally considered evidence for a metasomatic Group II origin (Calligaro *et al.* 1999; Muhlmeister *et al.* 1998), which may be totally appropriate for

the fluid-magmatic interaction of a granitic skarn. High Si has not been discussed in much detail, in part because Si has not been routinely analyzed, and if it has it was not discussed (*e.g.*, Tang et al. 1988). We hypothesize that the level of 150-500 ppm Si observed in Mogok belt corundum may well be within the solubility limits, but the sporadic analyses above that represent fine-scale inclusions, not visible by optical or most electron microscopy. However, the existence of this signature could well reflect the influence of silica infusion from the skarn formation process, not reflected in samples from other origins. The two Namya samples (109274-1,3), that also show the high Si (but normal Fe) content, may reflect the skarn origin without the Fe influx. Painite from Namya is relatively Fe poor compared to that from Wet Loo (bdl – 0.08 versus 0.1. – 0.23 wt% FeO, respectively; our data).

Other interpretations from the Mogok belt sample analysis

The compositions of the Mogok samples, even excluding Wet Loo, Dattaw, and certain Namya samples, have a greater range of compositions than expressed by the Group I boundaries of Calligaro *et al.* (1999). Figures 6B, 6C, and 7A clearly show low Fe and a considerable range in Cr content, which is not entirely new, as shown for a few analyses by Tang *et al.* 1988, Osipowicz *et al.* 1995, and Sanchez *et al.* 1997. Part of this greater range at low concentration may be due to the selection of pink corundum that does not qualify as ruby, sensu stricto, in the gem nomenclature.

The apparent clustering of samples from a particular locality with a band of V/Ti values (Fig. 8C) may have a genetic significance. Low V/Ti has been used as a distinguishing feature for Mongshu rubies in comparison to other marble-hosted samples from Myanmar. However, Dattaw, Kyauksin, and Kadoke Tat compositions clearly cluster in different V/Ti windows with variable Cr contents. The source of these elements is considered to be derived from phyllosilicates (clays and micas) in the impure zones in the marble (formerly limestone) (*e.g.*, Garnier *et al.* 2008). The primary sources of V and Cr, along with a host of transition metals,

453 are modeled as being derived from high molecular-weight organic molecules that scavenge
454 these elements from seawater and sediment pore fluids (*e.g.*, Lewan 1981, Schultz 1991).
455 Depending on inputs into the shallow basins where these organic-laden sediments form and
456 their subsequent reactions based on total carbon, sulfur content, permeability, etc., it is likely
457 that Eh-pH relations will locally retain or expel certain elements based on their solubility and
458 retention by organics and interacting clay minerals. This should lead to varying amounts of Cr
459 and V and other transition elements being retained in the sediment, while Ti, with an even
460 higher field strength, may be less subject to variation, as well as the observation that it is
461 correlated with detrital rather than organic sediment (Schultz 2004). With diagenesis and low-
462 grade metamorphism, Cr, V, and Ti are sequestered in illite – hydromuscovite rather than the
463 organic component in black shales (*e.g.*, Meyer and Robb 1996; Peacor, *et al.* 2000) while many
464 other elements are either lost or sequestered in sulfides or phosphates (Schultz 1991, 2004). So,
465 the V/Ti continuity in rubies from a single source in the Mogok belt may reflect some such local
466 geochemical signature in the limited extent of shale within the hosting marble and the
467 compatibility of these elements in corundum. Clearly, a deeper analysis is required to test this
468 hypothesis. Cu has been found above detection limits in marble-hosted ruby (Osipowicz *et al.*
469 1995; Sanchez *et al.* 1997; Rankin *et al.* 2003) and may be a reflection of other aspects of the
470 metal-rich black shale geochemistry. Our limited look at some of these elements did not yield
471 reliable results above the detection limit for Cu, Zn, or Sn, except for the apparent Cu-rich
472 sulfide in specimen 108498-1 from Kadoke Tat. Finally, the observation that red corundum can
473 have significant Ti, even greater than Cr + V, is clearly tied to the relatively low amount of iron,
474 as the latter (as Fe^{2+}) with Ti leads to a strong blue color via Fe^{2+}–Ti^{4+} intervalence charge
475 transfer absorption, as has been noted in research on Mongshu rubies (Peretti *et al.* 1995).

CONCLUSIONS

Trace element compositions measured in this study show somewhat distinctive ranges among the sources available, although the resolution is not sufficient to be useful for the kind of "determination of source" analysis desired by gemological laboratories. There is an overlap into the "metasomatic" Group II field (Calligaro *et al.,* 1999) from Group I, marble-hosted metamorphic ruby, more obvious in the Cr-V plot than in the Cr-Fe plot. However, the latter is probably a better discriminator as noted below. The trend of composition to lower Cr content that otherwise track with Group I probably relates to our choice of pink as well as red corundum for the study. Finally, the existing group boundaries of a single or pair of plots are inadequate even for our samples, all sourced from the Mogok Belt. Nonetheless, the majority of sources, excluding Wet Loo and perhaps parts of Sagyin, fall within the Group I field in both plots. Data from trapiche ruby samples from Mongshu cluster among published values for this source, so clearly they are uniformly distinguishable from Mogok belt samples.

The results of this study were unable to determine distinctive compositions for metamorphic versus skarn-related rubies, rather skarn-related rubies appear to have compositions much like other metasomatically formed ones. Samples from a skarn paragenetic setting, Wet Loo and possibly Dattaw and Namya, do not contain the skarn-critical elements B and Zr uniformly above the detection limits by LA-ICPMS with our analytical setup (or by EPMA). However, these samples did show higher Fe content, often associated with a metasomatic origin, as well as high Si. As, skarn formation is, in essence, a metasomatic process, it appears to provide a similar fingerprint of Fe content as a discriminant, at least with the examples studied here. Thus, the chemical system of the low-Fe rubies, characteristic of the marble-hosted metamorphic, is more depleted in Fe than the fluids evolving from the leucogranites in the Mogok Tract. Unfortunately, Si is not reported in the literature on metasomatically formed rubies to provide a comparison with the data here. Greater analytical

sensitivity for B, Zr, and perhaps other elements is necessary to evaluate whether another skarn signature is present.

Finally we offer a recommendation for improving connectivity between the gemological and geological literatures. The tendency in the gemological literature to provide inadequate descriptions of analytical techniques and samples as well as only summaries of compositional data as averages and ranges makes these data extremely limited for geological interpretation of the processes that crystallize gem minerals and give them individual identity. Clearly, this information is almost looked upon as proprietary because of its commercial value to testing laboratories. However, most labs contain similar data sets, so revealing this information is unlikely to affect business but could enhance scientific understanding and aid in exploration for new gem resources.

ACKNOWLEDGEMENTS

This research was made possible through generous support from the National Science Foundation for the AMNH REU program (AST 1004591) in Physical Sciences through which WB carried out a portion of this research. We are grateful for the assistance of Louise Bolge in the joint Lamont Doherty Earth Observatory (Columbia University) – AMNH LA-ICPMS facility. The manuscript was improved by the thoughtful reviews of Gaston Giuliani and George R. Rossman, as well as the editorial handling by Daniel Harlov.

REFERENCES

Abduriyim, A. and Kitawaki, H. (2006a) Determination of the origin of blue sapphire using Laser Ablation Inductively Coupled Plasma Mass Spectrometry (LA-ICP-MS). Journal of Gemmology, 30, 23-36.

525 Abduriyim, A. and Kitawaki, H. (2006b) Applications of Laser Ablation-Inductively Coupled
526 Plasma-Mass Spectrometry (LA-ICP-MS) to Gemology: Gems and Gemology, 42 (2),
527 98-118.
528 Bertrand, G. and Rangin, C. (2003) Tectonics of the western margin of the Shan plateau (central
529 Myanmar): implication for the India–Indochina oblique convergence since the
530 Oligocene. Journal of Asian Earth Sciences, 21, 1139-1157.
531 Bertrand, G., Rangin, C., Maluski, H., Bellon, H., [the GIAC Scientific Party] (2001)
532 Diachronous cooling along the Mogok Metamorphic Belt (Shan Scarp, Myanmar): the
533 trace of the northward migration of the Indian syntaxis. Journal of Asian Earth Sciences,
534 19, 649–659.
535 Bertrand, G., Rangin, C., Maluski, H., Han, T.A., Thein, M., Myint, O., Maw, W. and Lwin, S.
536 (1999) Cenozoic metamorphism along the Shan scarp (Myanmar): evidences for ductile
537 shear along the Sagaing fault or the northward migration of the eastern Himalayan
538 syntaxis? Geophysical Research Letters, 26, 915-918.
539 Calligaro, T., Mossman, A., Poirot, J.-P. and Querré, G. (1998) Provenance study of rubies from
540 a Parthian statuette by PIXIE analysis. Nuclear Instruments and Methods in Physics
541 Research B, 136-138, 846-850.
542 Calligaro, T., Poirot, J.-P. and Querré, G. (1999) Trace element fingerprinting of jewelry rubies
543 by external beam PIXE. Nuclear Instruments and Methods in Physics Research B, 150,
544 628-634.
545 Deer, W.A., Howie, R.A. and Zussman, J. (1982) Humite Group. In Rock-forming Minerals,
546 Vol. 1A, Orthosilicates, p. 379-417, Halsted Press, New York.
547 Garnier, V., Giuliani, G., Ohnenstetter, D., Fallick, A.E. Dubessy, J., Banks, D., Vinh, H.Q.,
548 Lhomme, T., Maluski, H., Pêcher, A., Bakhsh, K.A., Long, P.V., Trinh, P.T. and

549 Schwarz, D. (2008) Marble-hosted ruby deposits from Central and Southeast Asia:
550 Towards a new genetic model. Ore Geology Review, 34, 169-191.
551 Garnier. V., Maluski, H., Giuliani, G., Ohnenstetter, D. and Schwarz, D. (2006) Ar-Ar and U-
552 Pb ages of marble-hosted ruby deposits from central and southeast Asia. Canadian
553 Journal of Earth Sciences, 43, 509-532.
554 Garnier. V., Ohnenstetter, D., Giuliani, G., Blanc, P. and Schwarz, D. (2002) Trace-element
555 contents and cathodoluminescence of "trapiche" rubies from Mong Hsu, Myanmar
556 (Burma): geological significance. Mineralogy and Petrology, 76 (3-4), 179-193.
557 Giuliani, G., Ohnenstetter, D., Garnier, V., Fallick, A.E., Rakotondrazafy, M. and Schwarz, D.
558 (2007) The geology and genesis of gem corundum deposits, *in* Groat, L.A., ed., Geology
559 of Gem Deposits, Mineralogical Association of Canada Short Course 37: Quebec,
560 Canada, Mineralogical Association of Canada, p. 23-78.
561 Giuliani, G., Ohnenstetter, D., Fallick, A.E., Groat, L.A. and Feneyrol, J. (2012) Geographic
562 origin of gems tied to their geological history. In Color, 19 (1), 16-27.
563 Guillong, M. and Gunther, D. (2001) Quasi ‘non-destructive’ laser ablation-inductively coupled
564 plasma-mass spectrometry finger printing of sapphires. Spectrochimica Acta Part B, 56,
565 1219-1231.
566 Harlow, G.E., Pamukcu, A., Naung U, S. and Thu, K. (2006) Mineral assemblages and the
567 origin of ruby in the Mogok Stone Tract, Myanmar. Gems and Gemology, 42 (3), 147.
568 Harlow, G.E., Sahm, E. and Hunt, J. (2005) CL in support of interpreting gem deposits.
569 Goldschmidt 2005, Abstracts, A594.
570 Hughes, R.W. (1997) Burma (Myanmar). In Ruby & Sapphire, p. 300-343511 p. RWH
571 Publishing, Boulder, CO.
572 Hutchinson, C.S. (1989) Geological Evolution of South-East Asia, 368 p. Oxford University
573 Press, New York.

574 Iyer, L.A.N. (1953) The geology and gem-stones of the Mogok Stone Tract, Burma. Memoirs of
575 the Geological Survey of India, 82, 100p.
576 Kane, R.E. and Kammerling, R.C. (1992) Status of ruby and sapphire mining in the Mogok
577 Stone Tract. Gems and Gemology, 28, 152-174.
578 Lewan, M.D. (1984) Factors controlling the proportionality of vanadium to nickel in crude oils.
579 Geochimica et Cosmochimica Acta, 48, 2231-2238.
580 Meyer, F.M. and Robb, L.J. (1996) The geochemistry of black shales from the Chuniespoort
581 Group, Transvaal sequence, eastern Transvaal, South Africa. Economic Geology, 91,
582 111-121.
583 Mitchell, A.H.G. (1981) Phanerozoic plate boundaries in mainland SE Asia, the Himalayas and
584 Tibet. Journal of the Geological Society, London, 138, 109-122.
585 Mitchell, A.H.G. (1989) The Shan Plateau and western Burma, Mesozoic plate boundaries
586 correlation with Tibet. In A.M.C. Sengör, Ed., Tectonic Evolution of the Tethyan
587 Regions, p. 567-583 Proceedings of the NATO Advanced Study Institute, Istanbul,
588 1985.
589 Mitchell, A.H.G. (1992) Late Permian-Mesozoic events and the Mergui Group nappe in
590 Myanmar and Thailand. Journal of Southeast Asian Earth Sciences, 7, 165-178.
591 Mitchell, A.H.G. (1993) Cretaceous–Cenozoic tectonic events in the western Myanmar
592 (Burma)–Assam region. Journal of the Geological Society of London, 150, 1089-1102.
593 Muhlmeister, S., Fritsch, E., Shigley, J.E., Devouard, B. and Laurs, B.M. (1998) Separating
594 natural and synthetic rubies on the basis of trace-element chemistry. Gems and
595 Gemology, 34, 80-101.
596 Nissinboim, A. and Harlow, G.E. (2011) A study of ruby on painite from the Mogok Stone
597 Tract: Gems & Gemology, Research Track, Gem Localities and Formation, 47 (2), 140-
598 141.

599 Osipowicz, T., Tay, T.S., Orlic, I., Tang, S.M. and Watt, F. (1995) Nuclear microscopy of
600 rubies: trace elements and inclusions. Nuclear Instruments and Methods in Physics
601 Research B, 104, 590-594.
602 Peacor, D.R., Coveney, R.M. and Zhao, G. (2000) Authigenic illite and organic matter: the
603 principal hosts of vanadium in the Mecca Quarry shale at Velpen, Indiana. Clays and
604 Clay Minerals, 48, 311-316.
605 Peretti, A., Schmetzer, K., Bernhardt, H.-J. and Mouawad, F. (1995) Rubies from Mong Hsu.
606 Gems and Gemology, 31, 2-26.
607 Pouchou, J.L. and Pichoir, F. (1991) Quantitative analysis of homogenous or stratified
608 microvolumes applying the model "PAP". In K.F.K. Heinrich and D.E. Newbury, Eds., ,
609 p. 31-75Electron Probe Quantitation. New York, Plenum Press.
610 Rankin, A.H., Greenwood, J. and Hargreaves, D. (2003) Chemical fingerprinting of some East
611 African gem rubies by Laser Ablation ICP-MS: The Journal of Gemmology, 28 (8),
612 473-482.
613 Rossman, G.R. (2009) The geochemistry of gems and its relevance to gemology: Different
614 traces, different prices. Elements, 5 (3), 159-162.
615 Rossman, G.R., Nuang, S., Harlow, G.E. and Hunt, J. (2005) Painite ($CaZrBAl_9O_{18}$); a second
616 source in Myanmar and metasomatic origins: Geochimica et Cosmochimica Acta, 69, i.
617 10, 278.
618 Sanchez, J.L., Osipowicz, T., Tang, S.M., Tay, T.S. and Win, T.T. (1997) Micro-PIXE analysis
619 of trace element concentrations of natural rubies from different locations in Myanmar.
620 Nuclear Instruments and Methods in Physics Research B, 130, 682-686.
621 Schultz, R.B. (1991) Metalliferous black shales: accumulation of carbon and metals in cratonic
622 basins. Reviews in Economic Geology, 5, 171– 175.

623 Schultz, R.B. (2004) Geochemical relationships of Late Paleozoic carbon-rich shales of the
624 Midcontinent, USA: a compendium of results advocating changeable geochemical
625 conditions. Chemical Geology, 206, 347-372.
626 Schwarz, D., Pardieu, V., Saul, J.M., Schmetzer, K., Laurs, B.M., Guliani, G. Klemm, L.,
627 Malsy, A-K., Erel, E., Hauzenberger, C., Du Toit, G., Fallick, A.E. and Ohnenstetter, D.
628 (2008) Rubies and sapphire from Winz, Central Tanzania. Gems & Gemology, 44(4),
629 322-347.
630 Schwarz, D. and Schmetzer, K., (2001) Rubies from the Vatomandry area, eastern Madagascar.
631 Journal of Gemmology, 27 (7), 409-416.
632 Searle, D.L. and Haq, B.T. (1964) The Mogok belt of Burma and its relationship to the
633 Himalayan orogeny. In: Report of the 22nd Session, India, 1964, Part XI, Proceedings
634 of Section 11: Himalayan and Alpine Orogeny (eds. G. Kohli, V.S. Krishnaswamy, and
635 K.S. Valdiya). International Geological Congress, New Delhi, pp. 132-161.
636 Shannon, R. D. (1976) Revised effective ionic radii and systematic studies of interatomic
637 distances in halides and chalcogenides. Acta Crystallographica, A32, 751-757.
638 Sparks, J. (2001) A Excel program for processing ICP-MS data. Boston University.
639 Sutherland, F.L., Schwarz, D., Jobbins, E.A., Coenraads, R.R. and Webb, G. (1998) Distinctive
640 gem corundum suites from discrete basalt fields: comparative study of Barrington,
641 Australia, and West Pailin, Cambodia, gemfields: Journal of Gemmology, 26 (2), 65-85.
642 Tang S.M., Tang, S.H. and Mok, K.F. (1989) A study of natural and synthetic rubies by PIXIE.
643 Applied Spectroscopy, 43 (2), 219-223.
644 Tang, S.M., Tang, S.H., Tay, T.S. and Retty, A.T. (1988) Analysis of Burmese and Thai rubies
645 by PIXE. Applied Spectroscopy, 42 (1), 44-48.
646 Tang, S.M., Tang, S.H., Tay, T.S. and Retty, A.T. (1991) Analysis of Burmese and Thai rubies
647 by PIXE. Gemological Digest, 3 (2), 57-62.

Themelis, T. (2008) *Gems and Mines of Mogok*: Los Angeles, A & T Publishing, 356 p.

Thu, K. (2007) The Igneous rocks of the Mogok Stone Tract; their distributions, petrography, petrochemistry, sequence, geochronology and economic geology. Ph.D. Thesis, Yangon University, Yangon, Myanmar, 139 p.

FIGURE CAPTIONS

Figure 1: A political map showing northern Myanmar and the localities producing rubies as well as the Jade Tract center at Hpakan, (after Kane and Kammerling 1992). Sources in the Mogok Stone Tract are shown in Fig. 2.

Figure 2: A geologic map of a section of the Mogok Stone Tract showing four localities for the samples used in this study (after Hughes 1997).

Figure 3: Images of several samples analyzed in this study. A: ruby 107643 from Dattaw; B: 109274-3 from Sagyin; and C: 109276-1 from Namya. Laser ablation groves (vertical) are visible on the polished surfaces with scan lengths of 1.7 mm (A), 2.5 mm (B), and 2.9 mm (C).

Figure 4: CL images of ruby crystals. A: Part of a wedge-sector of trapiche ruby (110343-1) from Mongshu. Subtle zoning in at least four bands paralleling the $11\bar{2}0$ crystal face (top right) are visible. B: Ruby 107643 (also shown in 3A) with the spectrometer window set at 670 nm. This is the emission wave-length for Cr, which shows bright a Cr-rich tip at left

671 edge. The bright curved area at center in an artifact of the CL mirror system at low
672 magnification.
673
674 Figure 5: (A) Photomicrograph of Mongshu trapiche ruby sample 110343-1, with ablation
675 transect groove extending from the upper-left edge of the crystal inwards. (B) Plot of the
676 raw ICPMS intensity for Cr (red) and Ti (blue) concentrations in terms of intensity (counts
677 per second). A high-Cr rim and increasing Ti towards the center are clearly evident. The
678 darker core of the trapiche crystal is likely the result of higher Ti. (C) Plot of EPMA results
679 for a traverse adjacent to the laser transect shown in (A), which shows comparable results.
680
681 Figure 6: Binary elemental compositional plots in elemental parts-per-million (ppm) by
682 weight for the Mogok belt corundum. (A) Fe vs. Si from EPMA results; (B) Cr vs. V for
683 both EPMA (top) and ICPMS (bottom) data with source Groups I (metamorphic), II
684 (metasomatic), and III (basaltic) from Calligaro *et al.* (1999) interpreted from their EPMA
685 data. Kadoke Tat sample 108503 plots distinctively at higher V with somewhat low Cr
686 values. (C) Cr vs. Ti for both EPMA (top) and ICPMS (bottom) with EPMA values for an
687 inferred Myanmar marble-hosted origin from Calligaro et al. (1999), Mongshu ruby from
688 Peretti *et al.* (1995), and Mongshu trapiche ruby from Garnier *et al.* (2002).
689
690 Figure 7: Binary elemental compositional plots. (A) Cr vs. Fe after Calligaro *et al.* (1999)
691 showing source Groups I, II, and III with their data from an inferred Myanmar marble-
692 hosted ruby and from the EPMA data in this study. In the same manner as in Fig. 6C, the
693 Mongshu data of Peretti *et al.* (1995) and Garnier *et al.* (2002) are also plotted. Data for
694 Groups I, II, and III are from Calligaro et al. (1998, 1999). The detection limit for Fe of ~
695 65 ppm is shown, but all non-zero Fe EPMA is plotted to avoid a hard edge to the plot. (B)

696 V vs. Fe for EPMA and other data as in (A). Group I is shown according to tables in
697 Calligaro *et al.* (1998, 1999) and to rubies from Thailand deposits (basalt-hosted) of Tang
698 *et al.* (1988).
699
700 Figure 8: Elemental plots (not normalized). (A) Ternary Fe-V-Ga plot after Muhlmeister *et*
701 *al.* (1998) on left [plot taken from Giuliani *et al.* 2007] with additional data from Calligaro
702 *et al.* (1998, 1999), Peretti *et al.* (1995), and Garnier *et al.* (2002) sorted according to
703 marble-hosted (upper group), Group II, and Group III, and, on the right hand side, EPMA
704 data from this study. (B) LA-ICPMS data for V vs. Ga on samples from this study showing
705 that Ga < V. (C) Ternary V-Cr-Ti plot with published data (Calligaro *et al.* 1998, 1999;
706 Peretti *et al.* 1995; Garnier *et al.* 2002) and LA-ICPMS data from this study on the left and
707 EPMA data on the right.
708
709 Table 1

Region	Locality	Samples	Catalog Numbers	Associated phases (inclusions = i or +i if also in assemblage)	Sample Type
Mogok Tract	Dattaw	1	107643	balliranioite, "mizzonite" (scapolite), sodalite, calcite, phlogopite(i)	marble-hosted
		1	108409	calcite, fluorapatite, halloysite, spinel	eluvial crystal
	Kadoke Tat	1	108498	calcite(+i), clinohumite, cancrite-group, pargasite, montmorillonite, pyrrhotite(+i), phlogopite(+i)	marble-hosted
		1	108502	calcite	eluvial crystal cluster
	Kyauksin	1	110351	calcite, scapolite	marble-hosted
	Wet Loo	2	112224, 112226	painite, foitite, margarite, zircon, baddeleyite, rutile	coated crystals from skarn
Sagyin	Sagyin	1	109270	calcite, clinohumite, pargasite, graphite?	marble-hosted
		5	112703 - 112707	112703-4 – baddeleyite; 112705 – pyrite; 12706 – titanite(i), zircon(i)	crystals from marble

Namya	Namya	5	109274 (3), 109276 (2)	109274-2 – apatite(i), pyrite(i), meionite?(i), rutile(i), titanite(i)	alluvial pebbles
	Sa Baw	1	109272-1	calcite(+i), clinohumite, pargasite	eluvial pebbles
		1	109272-2	titanite, zoisite(i)	eluvial pebbles
Mongshu	Mongshu	3	110343 (3)	110343-2 – calcite, hydrous Al-oxide between sectors	alluvial crystals?

710

711 For other tables see explicit Excel files

Table 2: EPMA ranges by sample											
Concentra-tions in ppm	**Elements**										
	Si	Ti	V	Cr	Ga	Mg	Mn	Fe	Zn	Ca	Na
Dattaw											
107643 Trv 1	125 - 283	86 - 260	53 - 239	bdl - 3689	bdl - 340	bdl - 82	bdl - 133	bdl - 237	bdl	bdl - 117	bdl
107643 Trv 2	125 - 218	82 - 158	56 - 116	bdl - 203	bdl - 205	bdl - 81	bdl - 153	bdl - 213	-	-	-
108409 Trv1	98 - 198	127 - 224	73 - 125	68 - 209	bdl - 254	bdl - 97	bdl - 184	bdl - 208	bdl	bdl	bdl - 167
108409 Trv2	139 - 275	75 - 146	70 - 125	473 - 882	bdl - 294	bdl - 77	bdl - 127	bdl - 210	-	-	-
Wet Loo											
112224 Trv 1	525 - 775	78 - 188	269 - 359	972 - 1287	bdl - 376	bdl - 83	bdl - 142	300 - 572	bdl - 484?	bdl - 119	bdl - 132
112224 Trv 2	288 - 402	130 - 261	197 - 517	720 - 1914	bdl - 281	bdl - 281	bdl - 129	315 - 595	-	-	-
112226 Trv 1	255-509	80 - 189	360 - 465	1160 - 1523	bdl - 336	bdl - 67	bdl - 208	401 - 1175	bdl	bdl	bdl - 139
112226 Trv 2	424 - 1020	91 - 880	51 - 1067	610 - 3539	bdl - 407	bdl - 104	bdl - 287?	157 - 865	bdl	bdl - 126	bdl - 245?
Kadoke Tat											
108498-1 Trv1	141 - 1367	bdl - 207	186 - 345	1225 - 4589	bdl - 353	bdl - 91	bdl - 150	bdl - 602	bdl - 647?	bdl	bdl
108498-1 Trv2	190 - 320	bdl - 116	186 - 366	1197 - 3978	bdl - 300	bdl	bdl - 239?	103 - 261	bdl - 432?	bdl - 900?	bdl - 169
108498-1 Trv 3	148 - 262	bdl - 171	174 - 275	1405 - 2364	bdl - 348	bdl - 68	bdl - 165	bdl - 644	bdl - 476	bdl	bdl - 203
108502-1 Trv1	187 - 304	bdl - 79	295 - 2634	180 - 1962	bdl - 330	bdl	bdl - 500?	bdl - 230	bdl	bdl - 192	bdl - 183
108502-1 Trv2	220 - 320	bdl - 141	350 - 1087	195 - 983	bdl - 223	bdl - 54	-	106 - 262	-	-	-
Kyauksin											
110351 Trv1	288 - 638	bdl - 131	169 - 276	86 - 211	bdl - 215	bdl - 35	-	130 - 214	-	-	-
110351 Trv2	280 - 1499	bdl - 78	156 - 227	99 - 272	bdl - 270	bdl - 19	-	102 - 247	-	-	-
Thabeikkyin											
1103343-1	142 - 358	bdl - 2450	830 - 1738	1306 - 2498	bdl - 191	bdl - 60	bdl - 389?	bdl - 174	bdl - 488?	bdl - 196	bdl - 130
1103343-2	202 - 495	170 - 1008	203 - 331	2559 - 3251	bdl - 166	bdl - 20	bdl - 373?	bdl - 151	bdl - 499?	bdl - 114	bdl - 175?
1103343-3	142 - 495	592 - 1658	428 - 532	5409 - 8169	bdl - 177	bdl - 60	bdl - 306?	bdl - 129	bdl - 468?	bdl	bdl
Sagyin											
109270	214 - 286	226 - 327	154 - 234	481 - 2668	bdl - 158	46 - 148	bdl - 362?	413 - 577	bdl	bdl	bdl
112703 Trv1	242 - 321	52 - 147	72 - 178	716 - 1078	bdl - 213	bdl - 99	bdl - 575?	bdl - 306	bdl - 664?	bdl	bdl
112704 Trv1	245 - 297	bdl - 108	155 - 231	1036 - 2547	bdl - 209	bdl - 32	bdl - 263?	143 - 250	bdl	bdl	bdl

112704 Trv2	241 - 327	bdl - 175	164 - 267	2162 - 3203	bdl - 222	bdl - 77	-	84 - 241	-	-	-
112705 Trv1	230 - 325	bdl - 144	134 - 192	571 - 1306	bdl - 262	bdl - 82	bdl - 342?	bdl - 208	bdl	bdl - 131	bdl
112705 Trv2	191 - 287	89 - 161	136 - 190	829 - 1005	bdl - 254	bdl - 77	-	84 - 241	-	-	-
112706	54 - 904	58 - 114	91 - 162	144 - 321	bdl - 708	bdl - 93	bdl - 139	bdl - 183	bdl - 587?	bdl	bdl
112707 Trv1	147 - 247	162 - 320	70 - 382	545 - 1081	bdl - 343	37 - 131	bdl - 278?	98 - 254	bdl	bdl	bdl
112707 Trv2	157 - 284	158 - 309	59 - 156	552 - 693	bdl - 170	34 - 122	-	74 - 282	-	-	-
Namya											
109274-1	82 - 1320	70 - 260	440 - 710	1748 - 2576	bdl - 139	bdl - 84	bdl - 424?	87 - 225	bdl	bdl	bdl
109274-2	176 - 370	bdl - 148	131 - 521	907 - 1066	bdl - 206	bdl	bdl - 263	128 - 234	bdl - 540?	bdl	bdl
109274-3	209 - 6081	121 - 198	629 - 779	6829 - 8779	bdl - 198	28 - 57	bdl - 298?	70 - 234	bdl	bdl	bdl
109276-1	133 - 224	bdl - 161	251 - 426	522 - 1163	bdl - 330	bdl - 61	bdl - 153	bdl - 208	bdl	bdl	bdl
109276-3	131 - 314	bdl - 474	286 - 387	3987 - 4264	bdl - 249	bdl - 51	bdl - 206	bdl - 154	bdl	bdl - 169?	bdl
Sa Baw											
109272-1	158 - 621	53 - 120	279 - 322	604 - 700	bdl	bdl - 82	bdl - 338?	bdl - 225	bdl	bdl	bdl - 188?
109272-2	194 - 507	61 - 100	101 - 524	842 - 2378	bdl - 191	bdl	bdl - 228?	bdl - 206	bdl - 589?	bdl	bdl
Typical S.D. (in ppm)	10	10	10	55	20	45	20 or 170‡	15	350	70	100
Detection Limits †											
Min	31	29	27	42	109	22	85	60	400	104	107
Max	39	49	45	71	191	70	200	155	615	200	234
† Detection limits depending on different run conditions and background levels, so the ranges are listed.											
‡ Mn was measured in two different schemes, the analyses that include Na, Ca, and Zn have the higher S.D.											

Comments on Zoning
High Cr at rim
unzoned
unzoned
unzoned
2 levels of Cr & V
2 levels of Cr & V
lower Cr,V & higher Ti,Mg at rim
higher Cr, V, Ti, Fe at rim
subtle Cr banding
subtle Cr banding
subtle Cr banding
Cr & V bands (Fe?)
V increases inward
unzoned
unzoned
strongly zoned: Cr,V,Ti,Mg
slightly zoned: Ti,Mg
moderately zoned: Ti,Mg,Ga,Cr-inv
a "high" Cr, low Ti band
no clear zoning
modestly zoned-higher Cr,V@core; clearly evident in photomicrograph

higher Cr,V,Ti@rim
slightly zoned-Cr@rim
Unzoned
higher Cr,V @rim
higher Cr @ rim
Unzoned
Unzoned
2 levels of Cr, V, Ti
Unzoned
2 levels of Cr, Fe & Mg?
Unzoned
Unzoned
slightly zoned-Cr,V,Ti

Table 3: LA-ICPMS Results

Concentrations in ppm					Elements					
6-fold radius (Å) *	0.45	0.605	0.615	0.62	0.64	0.64	0.72	0.725	0.74	
	Be	Ti	Cr	Ga	V	Ta	Zr	Mg	Zn	Other
Dattaw										
108409-1	bdl	161	121	32.2	97	bdl	bdl	bdl	bdl	
108409-1b	bdl	111	702	42.1	88	0.03	bdl	bdl	bdl	
107643-1a	1.4	103	105	32.7	64	bdl	bdl	bdl	bdl	
107643-1b	bdl	80	136	33.6	66	bdl	bdl	bdl	bdl	
Wet Loo										
112224a	bdl	143	1167	86.8	326	bdl	bdl	bdl	bdl	
112224b	1.9	122	958	75.8	237	bdl	bdl	bdl	bdl	
112226a	bdl	105	1165	88.5	309	bdl	bdl	bdl	bdl	
112226aHiCr	bdl	95	1384	99.9	380	bdl	bdl	bdl	bdl	
112226a-LoCr	bdl	90	968	77.1	266	bdl	bdl	bdl	bdl	
Kadoke Tat										
108498-1a	1.7	77	2963	118.6	246	bdl	bdl	bdl	bdl	
108498-1b	bdl	65	2304	140.4	243	0.01	bdl	bdl	bdl	
108498-1c LoCu	0.8	bdl	1721	137.2	150	0.01	bdl	bdl	22.3	
108498-1c HiCu	1.8	136	2035	142.0	232	0.01	bdl	189.7	36.4	Fe = 15807; Cu = 6233; Sn = 23.6
108502-1a	bdl	bdl	487	15.7	464	bdl	bdl	bdl	bdl	
108502-1b	0.9	205	292	19.7	626	0.08	1.9	bdl	7.4	Nb = 0.2
108502-1c	bdl	54	315	21.5	486	bdl	bdl	bdl	10.5	
108502-1a hi V	bdl	bdl	390	21.3	1472	bdl	bdl	bdl	bdl	
108502-1a hi Cr lo V	bdl	bdl	1313	10.8	174	bdl	bdl	bdl	bdl	
108502-1a med V lo Cr	bdl	bdl	136	15.6	397	bdl	bdl	bdl	bdl	
108502-1b hi Ti lo V Cr	bdl	580	61	12.9	326	0.81	7.5	25.0	19.7	Cu = 1.6; Nb = 0.4
108502-1b hi Cr lo Ti	1.5	92	610	14.7	298	bdl	bdl	bdl	36.4	
108502-1b hi Ti V med Cr	1.1	525	192	18.8	749	0.09	5.2	bdl	9.8	Nb = 1.1
Kyauksin										

110351-1a	bdl	bdl	157	29.2	132	bdl	bdl	bdl	bdl	
110351-1b	bdl	bdl	145	35.5	192	bdl	bdl	bdl	bdl	
Thabeikkyin										
110343-1a	1.0	859	14013	43.7	1105	bdl	bdl	bdl	bdl	
110343-1a lo Ti	4.0	39	15200	30.7	619	bdl	bdl	bdl	bdl	
110343-1a hi Ti	5.7	2162	19767	50.0	1392	0.06	bdl	bdl	bdl	
110343-2a	bdl	424	3348	45.2	252	bdl	bdl	bdl	bdl	Ca = 795; Ba = 0.8
110343-3a	1.0	1164	6551	39.2	377	bdl	bdl	bdl	bdl	
Sagyin										
109270-1a	bdl	173	1133	18.7	200	bdl	bdl	107.6	bdl	
109270-1b	0.7	239	521	12.2	125	bdl	bdl	144.9	bdl	Fe = 571
109270-1c	bdl	139	542	4.9	116	bdl	bdl	97.4	bdl	
109270-1d	bdl	113	739	3.9	116	bdl	bdl	64.5	bdl	
112703-1	bdl	78	785	22.1	90	bdl	bdl	bdl	bdl	
112704-1	bdl	51	1279	42.4	178	bdl	bdl	bdl	bdl	
112704-2	bdl	81	2456	26.3	162	bdl	bdl	bdl	8.5	
112705-1	0.5	74	825	30.7	123	bdl	bdl	bdl	bdl	Ba = 11.0
112705-2	bdl	78	786	31.9	122	bdl	bdl	bdl	bdl	
112706-1	bdl	64	190	5.2	105	bdl	bdl	bdl	bdl	
112707-1	bdl	175	509	23.3	77	0.01	bdl	bdl	bdl	
112707-2	bdl	211	678	33.9	124	bdl	bdl	81.3	bdl	
Namya										
109274-1	bdl	130	1982	36.1	489	bdl	bdl	bdl	bdl	
109274-1_end	bdl	190	1596	47.4	357	bdl	bdl	66.5	bdl	
109274-2a	bdl	79	5759	59.6	252	bdl	bdl	bdl	bdl	
109274-2b	bdl	214	5991	73.4	184	bdl	bdl	bdl	bdl	
109274-3a	0.9	100	6864	48.7	547	bdl	bdl	bdl	bdl	
109276-1a	bdl	206	700	60.5	331	bdl	bdl	bdl	bdl	
109276-1a Lo Ti	bdl	56	628	23.1	213	bdl	bdl	bdl	30.9	
109276-1a_hi_Ti	bdl	574	479	107.6	483	0.08	1.7	bdl	bdl	
109276-3a	bdl	314	3928	43.7	278	bdl	bdl	bdl	bdl	

109276-3a lo Ti	bdl	194	4026	56.4	285	bdl	bdl	bdl	bdl
109276-3a hi Ti	bdl	739	3431	51.5	254	bdl	bdl	bdl	bdl
109276-3a med Ti	bdl	411	3653	56.1	283	bdl	bdl	bdl	bdl
Sa Baw									
109272-1a	bdl	61	391	5.5	267	bdl	bdl	bdl	bdl
109272-2a	bdl	48	1030	31.1	198	bdl	bdl	bdl	bdl
109272-2a lo V Cr	bdl	40	750	35.1	90	bdl	bdl	bdl	bdl
109272-2a hi V Cr	bdl	59	1501	28.8	352	0.01	bdl	bdl	bdl
Standard Deviation	0.4	6	1	0.1	0.2	0.01	0.2	8	0.4
(in ppm)†	B=0.4, Si=140, Nb=0.04, Fe=47, Mn=0.6, Sn=0.1, Li=0.8, Cu=0.4, Ca=43, Ba=0.2								
Detection Limits	0.2–44	18–60	11–45	0.6–2.8	0.5–2.1	0.001–0.03	0.5–3.4	6–151	4–15
(in ppm)	B=3–39, Si=1400–6550, Nb=0.09–0.4, Fe=544–2332, Mn=3–155, Sn=2–8, Li=7–53, Cu=4–17, Ca=256–1573, Ba=0.2–1								

* Ionic radii from Shannon (1976); organized in increasing 6-fold radii to compare with Al = 0.535 Å

† Estimated from standards, given the low to below detection values in most samples, but realistically values should be at least several %

710 Figure 1

711

712

713

714

715 Figure 2

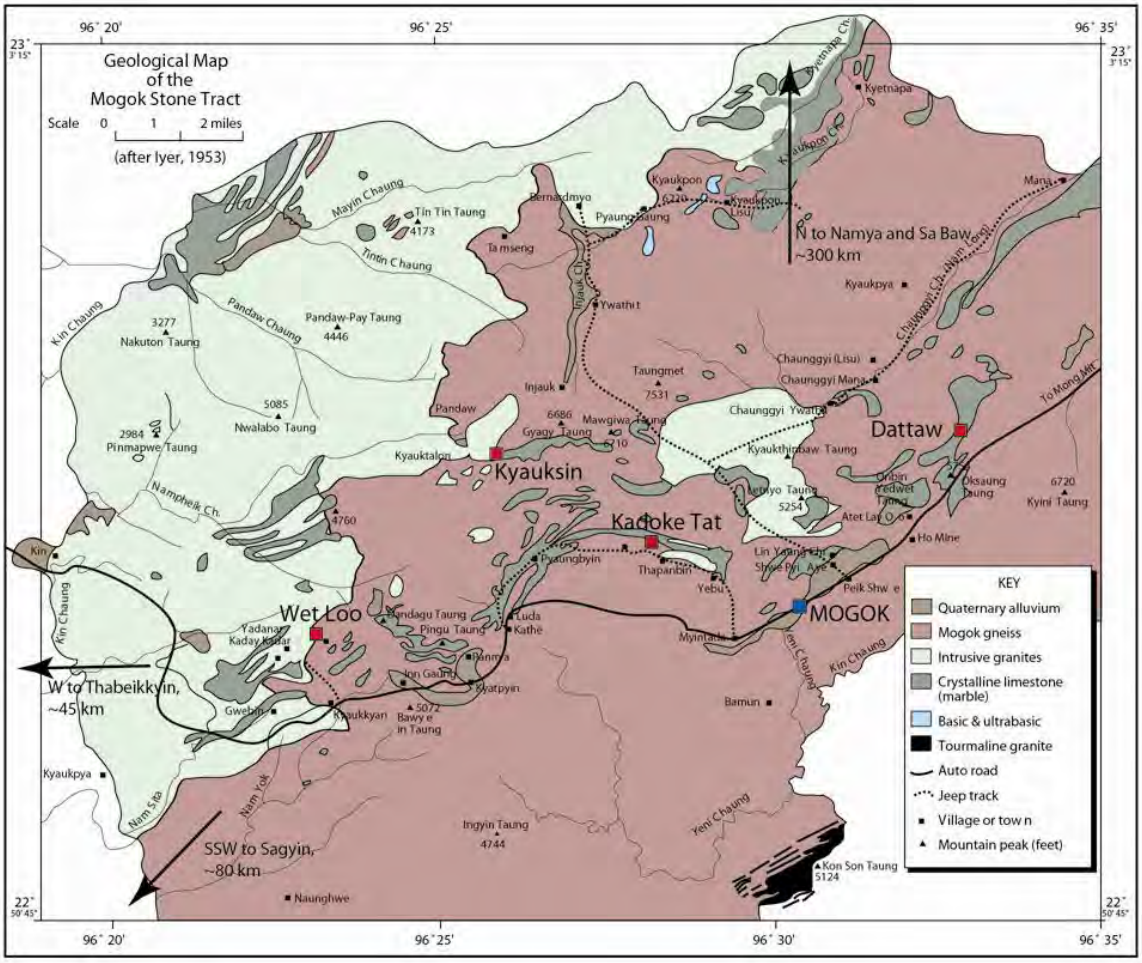

716

717

718 Figure 3

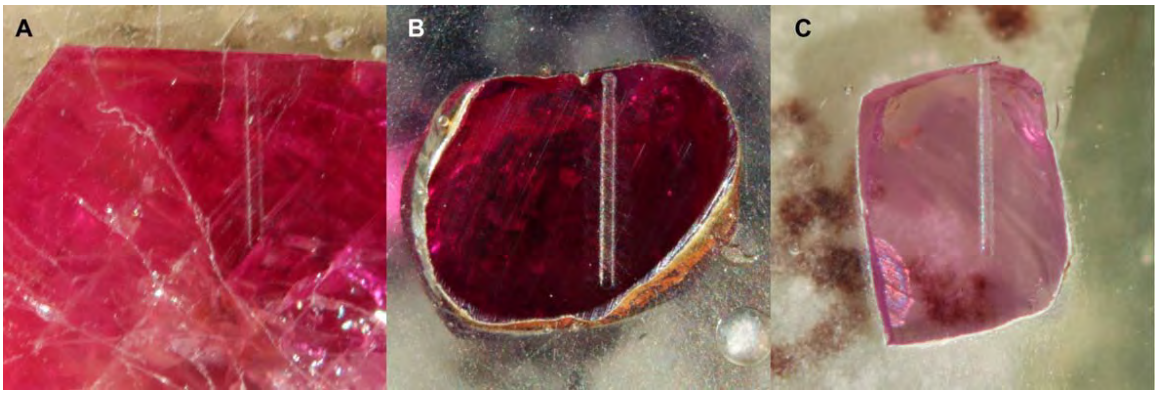

719

720

721 Figure 4

722 A

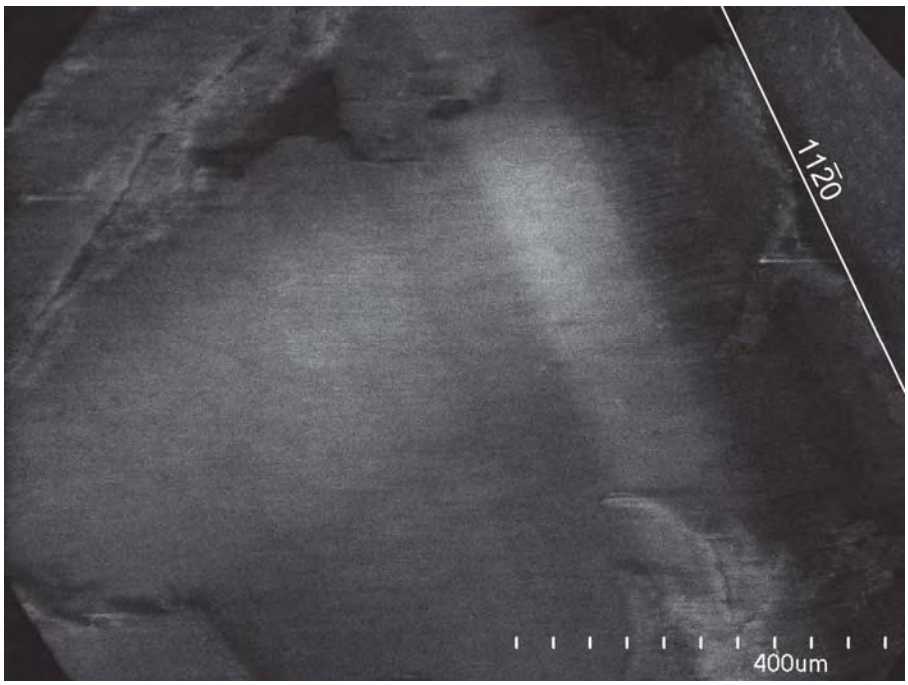

723

724 B

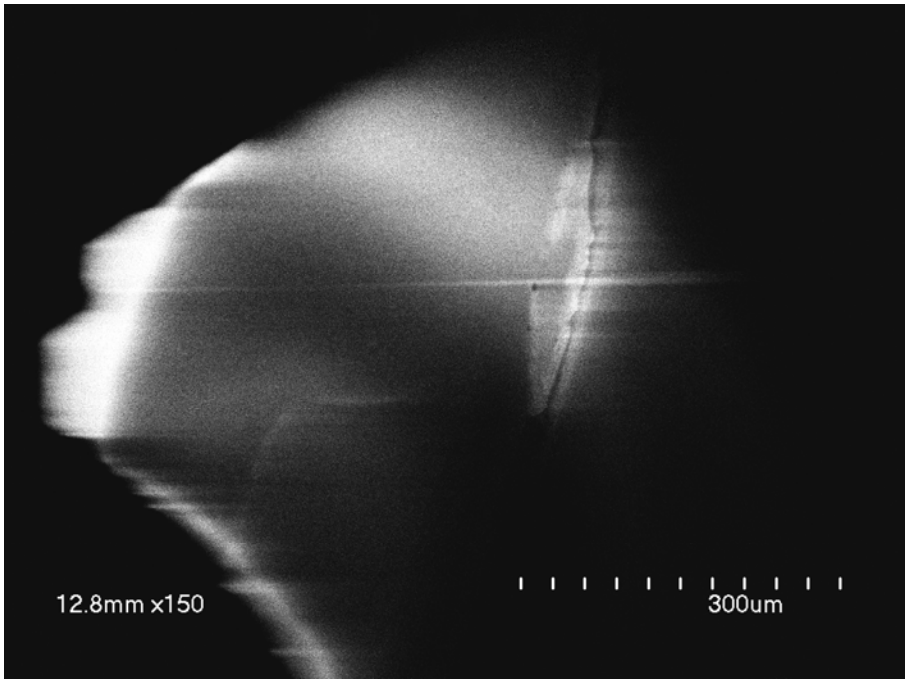

725

726

727 Figure 5

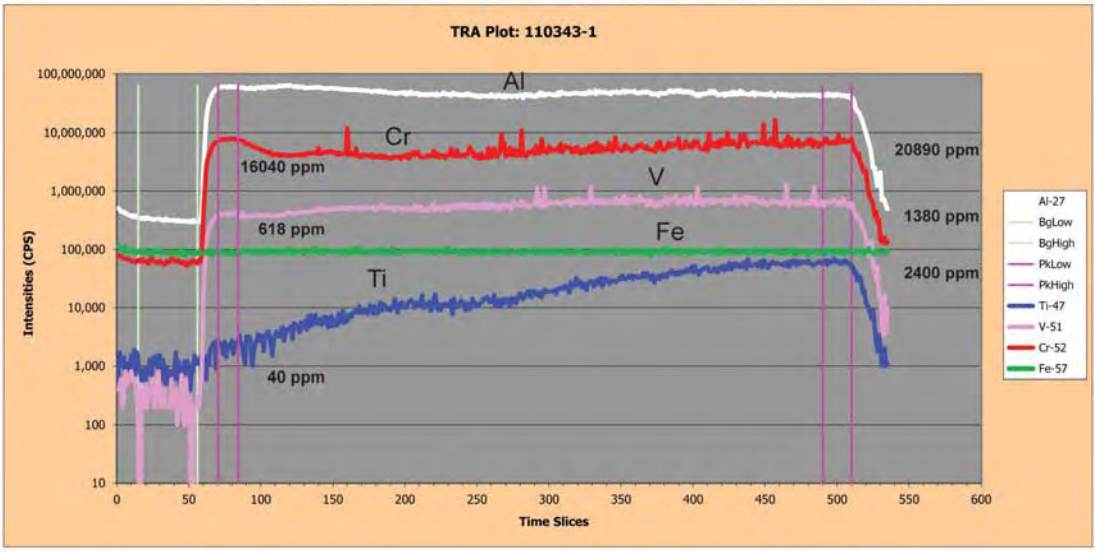

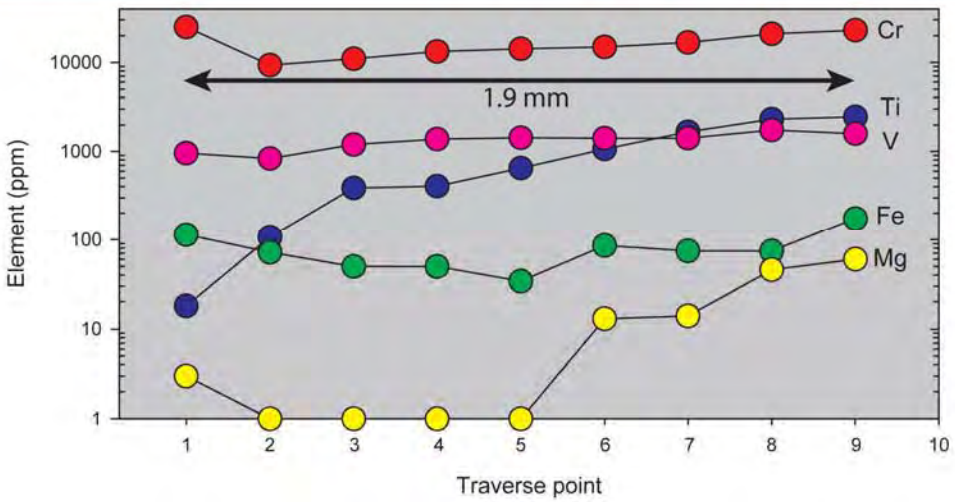

728

729

730 Figure 6A

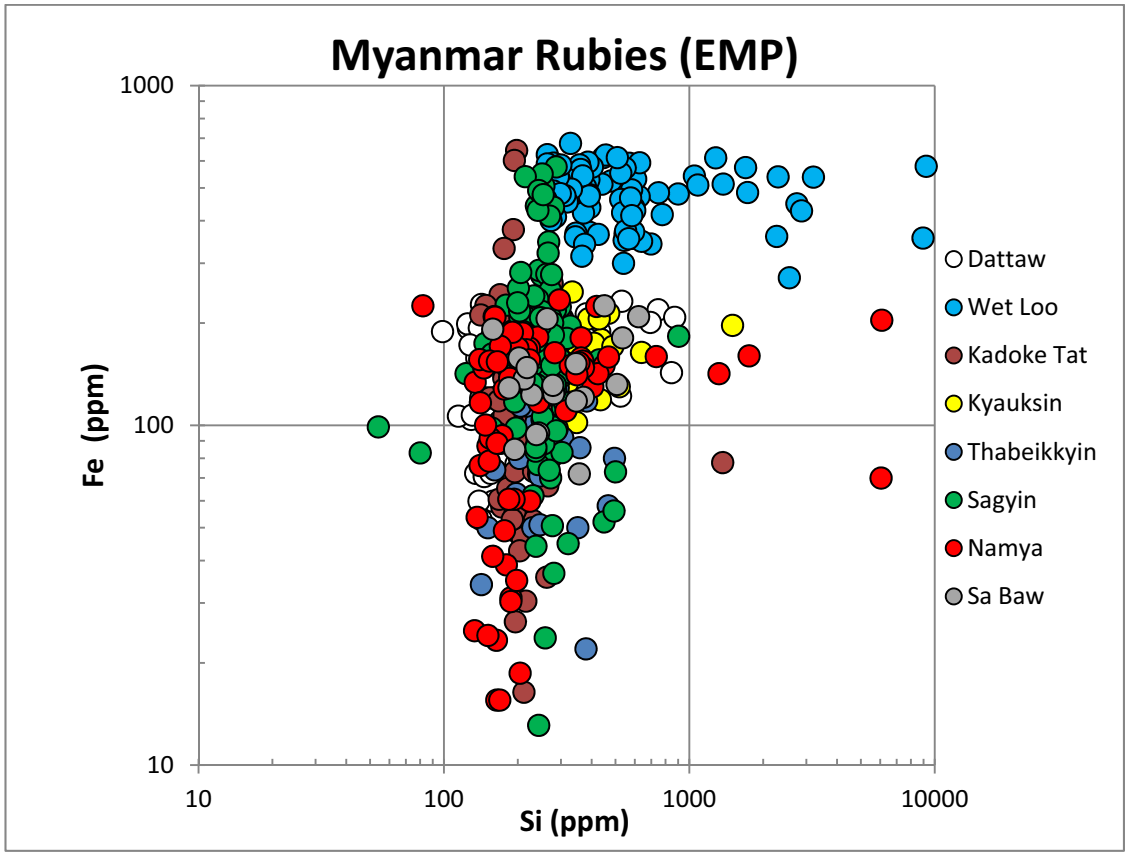

731

732

733

734 Figure 6B

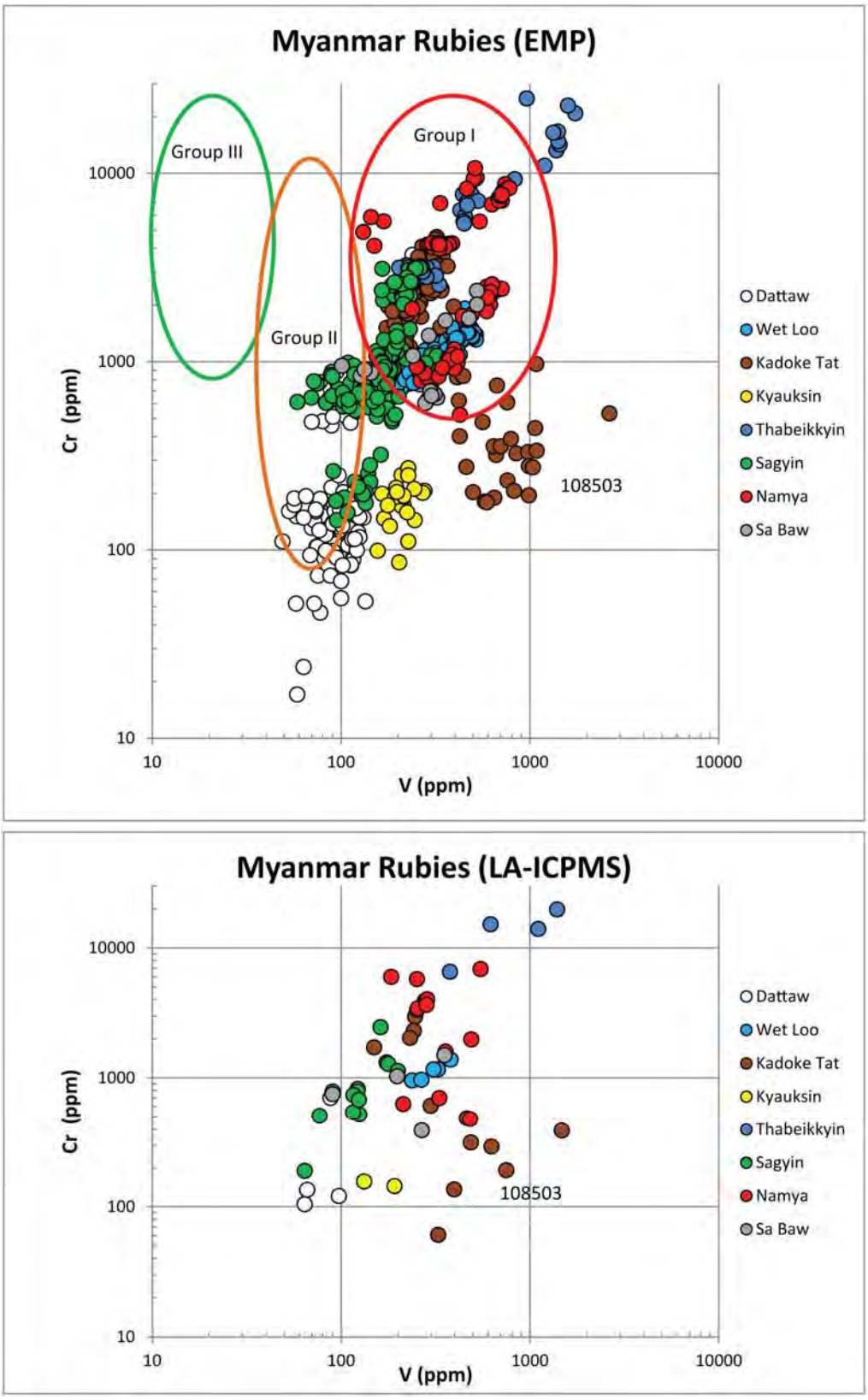

735

736

737 Figure 6C

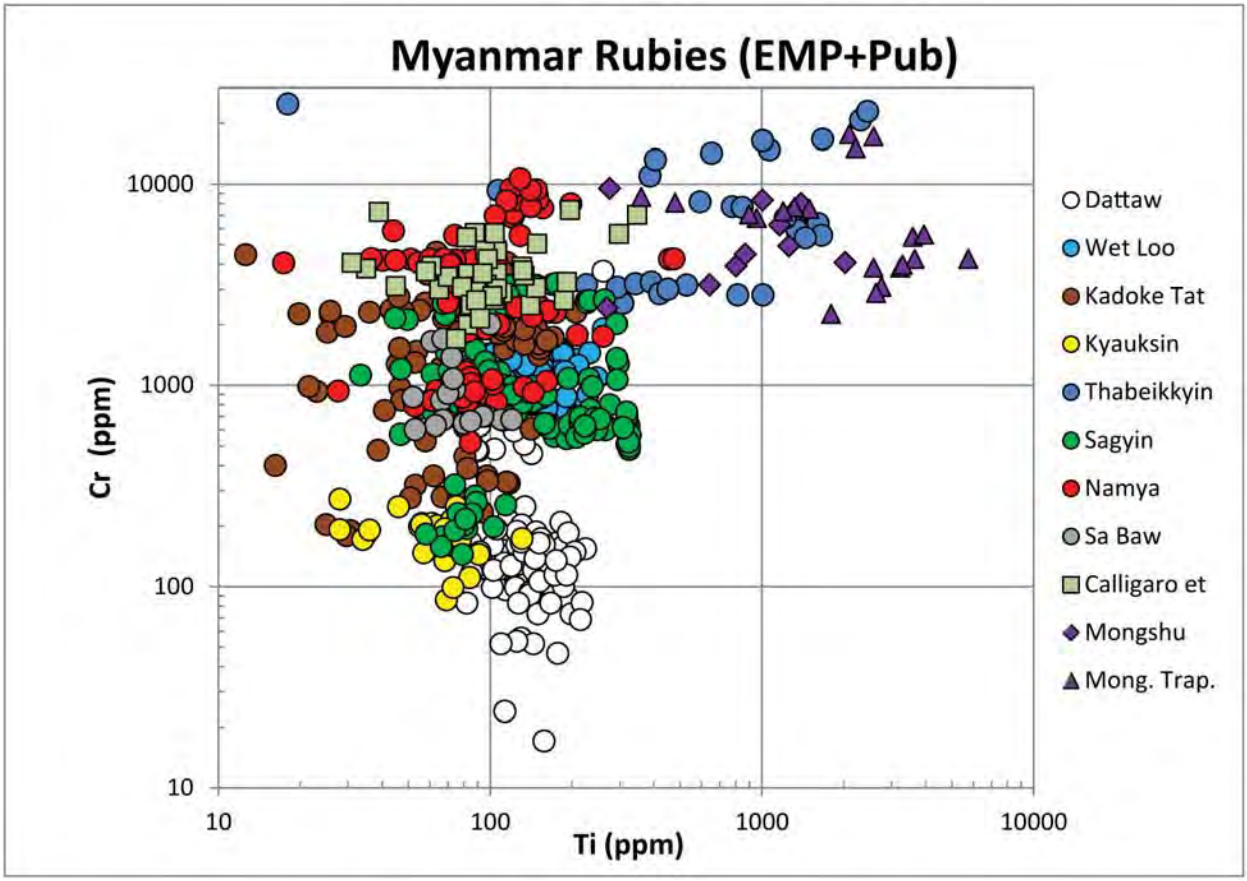

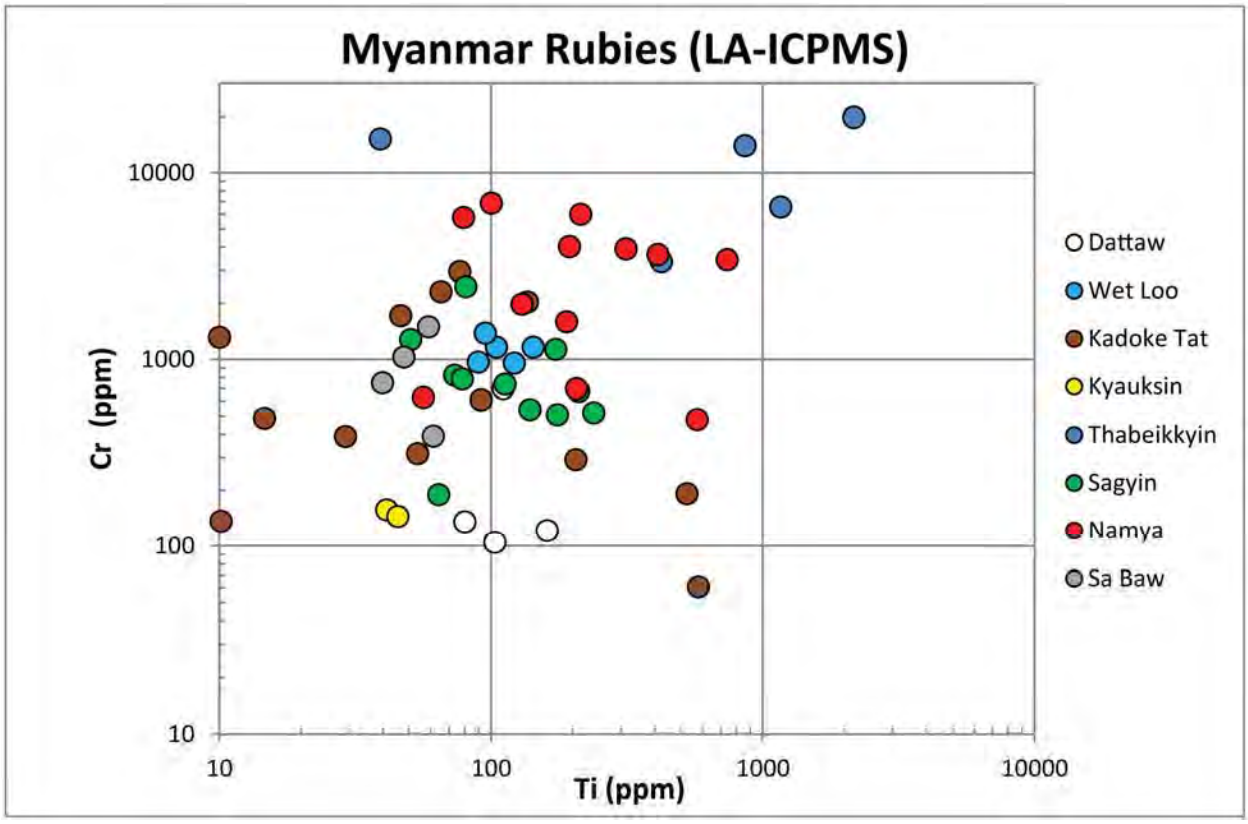

738

739 Figure 7

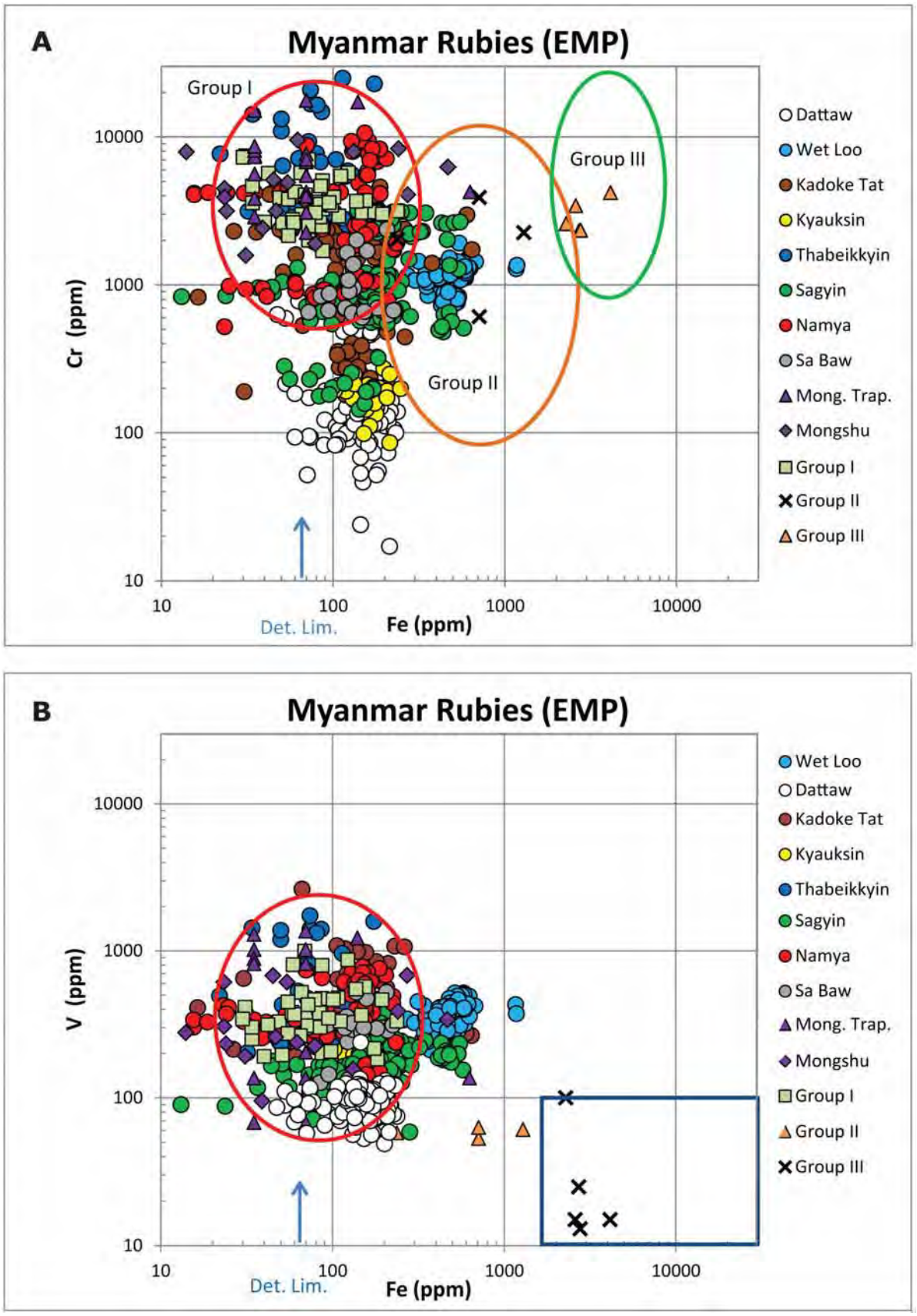

740

741 Figure 8A

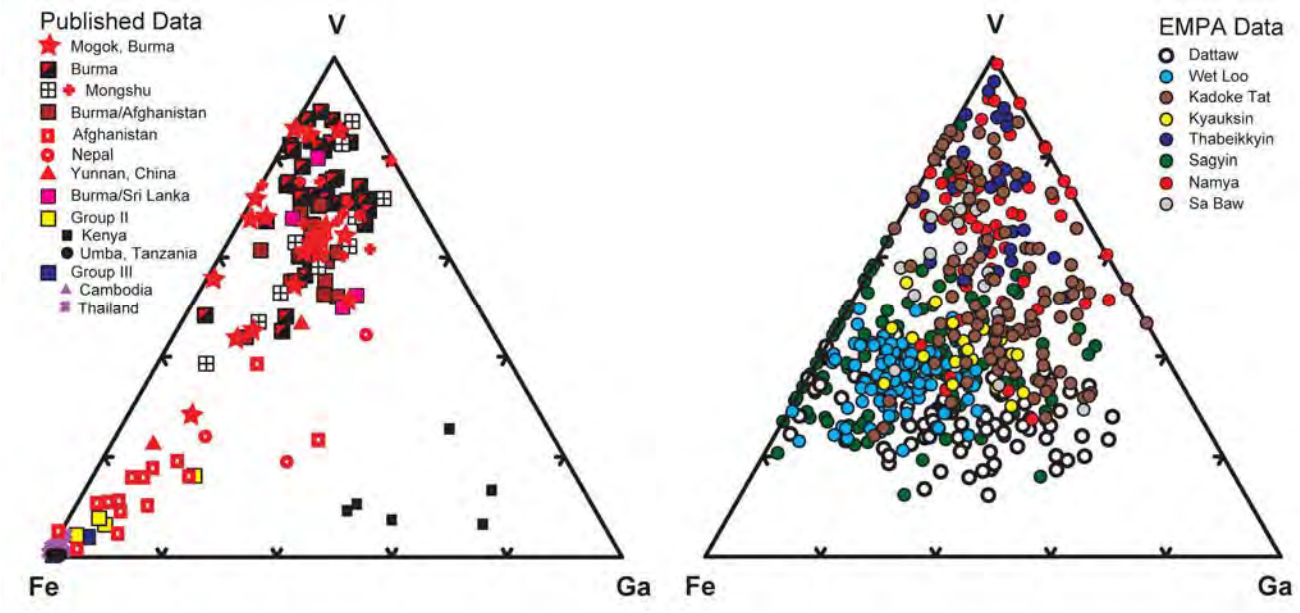

742

743

744 Figure 8B

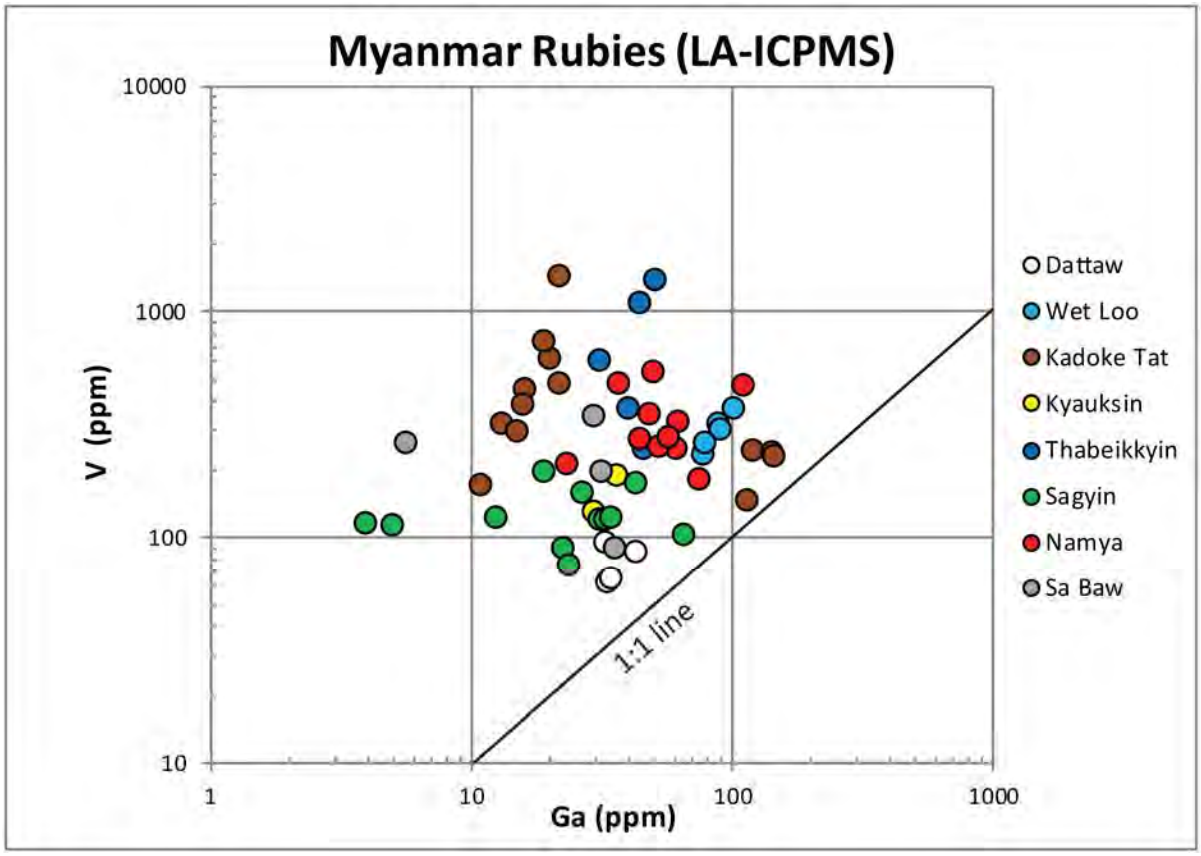

745

746

747 Figure 8C

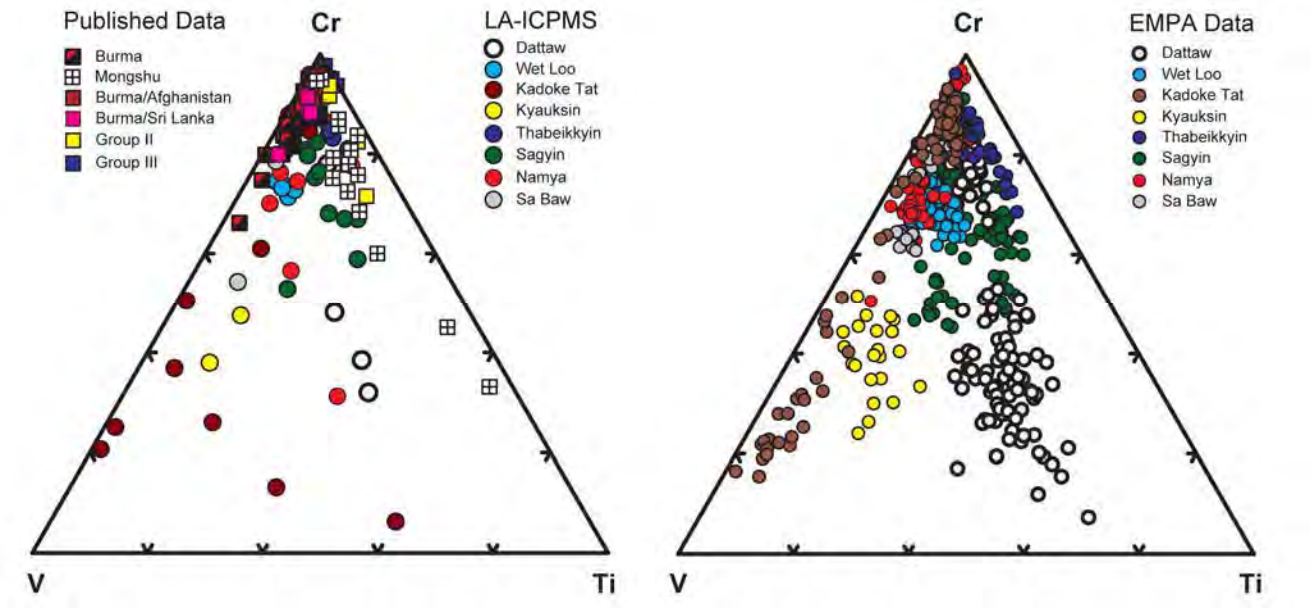

748

749